HHS Public Access

Author manuscript

Immunity. Author manuscript; available in PMC 2023 July 12.

Published in final edited form as:

Immunity. 2022 July 12; 55(7): 1234–1249.e6. doi:10.1016/j.immuni.2022.05.001.

Newly recruited intraepithelial Ly6A^{+}CCR9^{+}CD4^{+} T cells protect against enteric viral infection

Roham Parsa[1,8], **Mariya London**[1,3], **Tiago Bruno Rezende de Castro**[1,4], **Bernardo Reis**[1], **Julian Buissant des Amorie**[1,5], **Jason G. Smith**[6], **Daniel Mucida**[1,2,7,8]

[1]Laboratory of Mucosal Immunology, The Rockefeller University, New York, NY 10065, USA.

[2]Howard Hughes Medical Institute, The Rockefeller University, New York, NY 10065, USA.

[3]Present address: Department of Microbiology, New York University Grossman School of Medicine, New York, NY 10016, USA.

[4]Laboratory of Lymphocyte Dynamics, The Rockefeller University, New York, NY 10065, USA.

[5]Present address: Molecular Cancer Research, Center for Molecular Medicine, University Medical Center Utrecht, Utrecht University, The Netherlands.

[6]Department of Microbiology, University of Washington School of Medicine, Seattle, WA 98109, USA.

[7]Lead contact

Summary

The intestinal epithelium comprises the body's largest surface exposed to viruses. Additionally, the gut epithelium hosts a large population of intraepithelial T lymphocytes, or IELs, although their role in resistance against viral infections remains elusive. By fate-mapping T cells recruited to the murine intestine, we observed an accumulation of newly recruited CD4^{+} T cells after infection with murine norovirus CR6 and adenovirus type-2 (AdV), but not reovirus. CR6- and AdV-recruited intraepithelial CD4^{+} T cells co-expressed Ly6A and chemokine receptor CCR9, exhibited T helper 1 and cytotoxic profiles and conferred protection against AdV *in vivo* and in an organoid model in an IFN-γ-dependent manner. Ablation of the T cell receptor (TCR) or the

[8]Correspondence should be addressed to R.P. (rparsa@rockefeller.edu) or D.M. (mucida@rockefeller.edu), P. 212-327-7520.

Author contributions

R.P. designed and performed experiments and wrote the manuscript. R.P. and T.B.R.C. performed all bioinformatics analyses and T.B.R.C. assisted with interpretation of sequencing data. R.P. and M.L. performed sample and library preparation of bulk RNA-seq. R.P., M.L. and B.R. performed single-cell PCRs and multiplexing of samples for single-cell TCR-seq. M.L. and T.B.R.C. helped with analysis of single cell TCR-seq by MiSeq. R.P. and J.B.A. setup and performed organoid experiments. J.G.S. purified and provided WT and engineered adenovirus. D.M. conceived and supervised the research and wrote the manuscript. All authors edited the manuscript.

Declaration of interests

The authors declare no competing interests.

Inclusion and diversity statement

One or more of the authors of this paper self-identifies as an underrepresented ethnic minority in science. While citing references scientifically relevant for this work, we also actively working to promote gender balance in our reference list.

transcription factor ThPOK in CD4$^+$ T cells prior to AdV infection prevented viral control, while TCR ablation during infection did not impact viral clearance. These results uncover a protective role for intraepithelial Ly6A$^+$CCR9$^+$CD4$^+$ T cells against enteric adenovirus.

Graphical Abstract

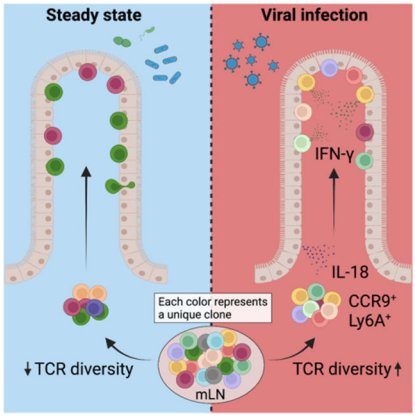

eTOC Blurb

It is known that a large number of T cells accumulate in the gut epithelium, but it remained unclear whether they play a role against enteric virus infections. Using fate-mapping models, Parsa et al. report that distinct enteric viruses induce the recruitment of CD4$^+$ T cells to the gut epithelium and that these cells control viral replication via IFN-γ secretion.

Introduction

The highly specialized intestinal immune system is charged with maintaining tolerance to harmless stimuli from commensal bacteria and food, while providing protective immunity against pathogens and epithelial cancers (Florsheim et al., 2021; Honda and Littman, 2016; McDonald et al., 2018; Tanoue et al., 2016). Intraepithelial lymphocytes (IELs) comprise a large T cell population located at the critical interface between the intestinal lumen and the core of the body. IELs can provide a first line of immunity in mice and humans, while balancing tolerance and defense (Bilate et al., 2020; Cervantes-Barragan et al., 2017; Edelblum et al., 2015; Hoytema van Konijnenburg et al., 2017; Jabri and Sollid, 2009; Sujino et al., 2016). Among the IEL populations, CD4$^+$ T cells are key players in intestinal homeostasis, finely tuning responses at the level of antigen recognition and functional differentiation. In the intestinal epithelium (IE) and underlying lamina propria (LP), tissue adapted pro-inflammatory, regulatory (Treg) and intraepithelial (CD8αα$^+$ CD4 IEL) CD4$^+$ T cells coordinate immunity and tolerance to diverse intestinal stimuli (Cervantes-Barragan *et al.*, 2017; Honda and Littman, 2016; McDonald *et al.*, 2018; Sujino *et al.*, 2016). Both LP and IE CD4$^+$ T cells are antigen-experienced and co-express markers of activation, gut-homing and tissue residency, including CD44, CD69, CD103 and CD8αα homodimers (Masopust and Soerens, 2019).

Enteric viruses, such as norovirus, rotavirus and adenovirus, are among the most common causes of acute gastroenteritis in humans and are responsible for morbidity and mortality worldwide (Iliev and Cadwell, 2021; Wilhelmi et al., 2003). These enteric viruses can infect intestinal epithelial cells and myeloid cells in the LP, provoking robust innate and adaptive immune responses (Iliev and Cadwell, 2021); however, a functional role for intestinal T cells in resistance to enteric viruses is not well established. We sought to address the functional role of intestinal T cells in the response to enteric viral infections by developing a T cell fate-mapping strategy to identify and characterize IE T cell dynamics during enteric viral infection. We observed specific recruitment and accumulation of $CCR9^{+}Ly6A^{+}CD4^{+}$ T cells, expressing a T helper 1 (Th1) and cytotoxic profile, in the epithelium after murine norovirus (MNV) CR6 and murine adenovirus-2 (AdV) infections. Virus-recruited $CD4^{+}$ T cells displayed increased T cell receptor (TCR) diversity while ablation of the TCR or the CD4-lineage defining transcription factor T-Helper-Inducing POZ/Krueppel-Like Factor (ThPOK) in $CD4^{+}$ T cells prior to AdV infection prevented viral control. In summary, we found that intraepithelial CD4+ T cells protect against enteric virus infection in a ThPOK- and IFN-γ-dependent manner.

Results

Enteric virus infection leads to distinct T cell dynamics

To characterize T cell dynamics in the IE during enteric viral infections, we infected mice with four different viruses, chronic MNV (CR6), acute MNV (CW3) (Strong et al., 2012), reovirus T1L (T1L) (Bouziat et al., 2017) and AdV (Wilson et al., 2017). CR6 infects intestinal tuft cells in the IE to establish long-lasting chronic infection (Graziano et al., 2021; Wilen et al., 2018), while CW3 and T1L infect multiple cell types including myeloid and stromal cells in the LP (Grau et al., 2017; Graziano *et al.*, 2021). AdV exclusively infects and replicates in the IE (Takeuchi and Hashimoto, 1976) (Figure S1A). We have previously shown that during steady state, $CD4^{+}$ T cells enter the IE as $CD103^{-}$ effector T cells and gradually acquire an IEL phenotype with progressive expression of CD103 and CD8αα (Bilate *et al.*, 2020; London et al., 2021). To understand T cell recruitment dynamics to the site of enteric infections, we first quantified the frequencies of $CD103^{-}$ T cells in the IE 10 days post infection by flow cytometry. We observed that AdV infection resulted in an increase of $CD4^{+}CD103^{-}$ T cells whereas T1L infection led to an increase in $CD8\alpha\beta^{+}CD103^{-}$ T cells in the IE (Figure 1A, B). To independently assess peripheral T cell recruitment to the IE during viral infections, we developed a fate-mapping approach. We crossed *Sell*^{CreERT2} (Merkenschlager et al., 2021) with *Rosa26*$^{CAG\text{-}LSL\text{-}tdTomato}$ ($iSell^{Tomato}$) to permanently label naïve T cells ($CD62L^{+}$) as $Tomato^{+}$ upon tamoxifen treatment, enabling a strategy that enriched for “ex-naïve” ($CD62L^{-}Tomato^{+}$) pathogen-specific T cells that migrated to the intestine (Figure 1C, S1B and S1C). Analysis of tamoxifen-treated $iSell^{Tomato}$ mice 10 days post infection revealed a significant increase of recently recruited ($Tomato^{+}$) $CD4^{+}$ T cells post AdV and CR6 infections, whereas T1L and CW3 infections led to a preferential recruitment of $CD8\alpha\beta^{+}$ T cells (Figure 1D, E and Figure S1D). Additionally, although all tested enteric viruses led to a significant recruitment of $CD4^{+}$ T cells to the LP, CW3, CR6 and T1L preferentially recruited $CD8\alpha\beta^{+}$ T cells to this compartment (Figure S1E and S1F).

We then focused on AdV infection as this virus preferentially recruited CD4$^+$ T cells and exclusively infects the intestinal epithelium. As expected based on a prior study, newly recruited CD4$^+$ T cells in response to AdV infection did not express typical IEL markers such as CD103, CD8αα or CD244 (Reis et al., 2013), but the majority of Tomato$^+$ T cells expressed CD69 indicating recent activation, or early tissue-residency (Faria et al., 2017) (Figure 1F, G and S1G). Using a fate-mapping strategy we revealed that the dynamics of recently recruited T cells differ between enteric viral infections.

Recruited intraepithelial CD4$^+$ T cells display a mixed Th1 and T cytotoxic profile

Next, we analyzed the gene expression profiles of newly recruited IE and LP CD4$^+$ T cells from AdV-infected mice. Unbiased clustering of the gene expression data and principal component analysis segregated CD4$^+$Tomato$^+$ T cells from infected mice in comparison to uninfected mice (Figure 2A, B). CD4$^+$Tomato$^+$ T cells from AdV infected mice displayed tissue specific gene expression such as *Ccl5* and *Itga1* in the IE, and *Fasl* and *IL12rb2* in the LP, indicating tissue adaptation and some degree of compartmentalization (London *et al.*, 2021). CD4$^+$Tomato$^+$ T cells from both compartments of AdV-infected mice displayed expression of inflammation- and gut residency-associated genes (*Ccr9*, *Ly6a*, *Lztfl1* and *Fyco1*), with a mixed Th1 (*Prdm1*, *Tbx21*, *Id2* and *Cxcr6*) and T cytotoxic (CTL) (*Runx3*, *Nkg7*, *Gzma* and *Gzmk*) profiles (Figure 2A, C and D). Overall, these results suggest that intestinal CD4$^+$ T cells recruited upon AdV infection display mixed Th1 and CTL profiles.

Our transcriptional analysis indicated a heterogenous profile of the recruited CD4$^+$ IE T cells post enteric AdV infection. To initially assess their functional profile, we infected tamoxifen-treated iSell^{Tomato} mice and characterized by flow cytometry CD4$^+$Tomato$^+$ T cells 10- and 30-days post AdV infection by using markers such as Ly6A and CCR9, enriched in our RNAseq data. As expected, we detected only a few fate-mapped CCR9$^+$Ly6A$^+$CD4$^+$ T cells in the IE and LP compartments in naïve uninfected mice. In contrast, AdV-infection significantly increased the recruitment of CCR9$^+$Ly6A$^+$CD4$^+$ T cells and granzyme B (GzmB) expression (Figure 3A). Additional cell surface markers with transcripts increased in the RNAseq analysis and associated with gut tissue recruitment during AdV-infection include CXCR6 and LFA-1 (CD11a/CD18) for the intraepithelial compartment, and CXCR3 for the LP. By day 30 post infection, no differences were observed in these surface markers between control and AdV-infected mice, while CCR9$^+$Ly6A$^+$, CXCR3$^+$ and LFA-1 remained increased in CD4$^+$Tomato$^+$ T cells isolated from the LP of AdV-infected mice, suggesting different retention or replacement dynamics between these compartments (Figure S2A and S2B).

The majority of recruited CD4$^+$Tomato$^+$ in AdV-infected mice expressed the transcription factor *Tbx21* (T-bet) (Figure 3B), associated with T_H1 phenotype as well as with IEL differentiation (Reis et al., 2014). Accordingly, we detected increased IFN-γ expression in CD4$^+$Tomato$^+$ IE T cells from AdV-infected mice in comparison to CD4$^+$Tomato$^+$ IE T cells isolated from uninfected mice (Figure 3C). CCR9$^+$Ly6A$^+$ T cells were the main IFN-γ producers within recruited Tomato$^+$ CD4$^+$ T cells (Figure 3D). Because we observed that different enteric viruses give rise to distinct T cell responses in the IE compartment (see Figure 1E above), we infected tamoxifen-treated iSell^{Tomato} mice with CR6 or T1L to

determine if these viruses could also induce CCR9^{+}Ly6A^{+}CD4^{+} T cells. In agreement with differences observed in the CD4 T cell recruitment between these viruses, CR6, but not T1L infection, led to increased CCR9^{+}Ly6A^{+}CD4^{+} T cells (Figure 3E) with similar GzmB expression as observed in AdV-recruited CD4^{+}Tomato^{+} T cells (Figure 3F). To address whether other enteric pathogens also induce CCR9 and Ly6A expression in newly recruited CD4^{+} T cells, we orally infected iSell^{Tomato} mice with *Listeria monocytogenes* 10403S-inlA. Listeria-specific IE CD4^{+}Tomato^{+} T cells upregulated Ly6A but failed to upregulate CCR9 (Figure S3A, B and C), pointing to pathogen-associated recruiting programs (Kiner et al., 2021). These results reveal that CR6 and AdV infections induce gut recruitment of CD4^{+} T cells expressing CCR9, Ly6A, and an overall Th1/CTL phenotype.

Recruited intraepithelial CD4^{+} T cells are clonally diverse and temporally TCR-dependent for controlling AdV-replication *in vivo*

To determine the role of the T cell receptor (TCR) in controlling AdV viral replication, we first extracted the TCR CDR3 sequences for both the α and the β chain from our bulk RNAseq data. Analysis of the CDR3 sequences suggested an increased number of reads for unique CDR3 sequences in CD4^{+} T cells recruited during acute viral infection in comparison to CD4^{+} T cells recently recruited in naïve mice (Figure 4A). We have recently shown that CD4^{+} T cells in the IE undergo clonal selection and reduction in TCR diversity as cells differentiate from conventional CD103^{-} CD4^{+} T cells into differentiated CD103^{+}CD8αα^{+} CD4^{+}IELs (Bilate *et al.*, 2020). To further investigate the TCR repertoire of AdV-recruited IE CD4^{+} T cells, we infected tamoxifen-treated iSell^{Tomato} mice with AdV and sequenced the TCRβ chain of single cell sorted Tomato^{+} CD4^{+} T cells, 10- and 30-days post-infection (AdV) or post-PBS injection (PBS). As shown earlier, most of the Tomato^{+} CD4^{+} T cells from AdV-infected mice were Ly6A^{+}, whereas Tomato^{+} CD4^{+} T cells in uninfected mice were mostly Ly6A^{-} (Figure 4B). Analysis of newly recruited (Tomato^{+}) Ly6A^{-} CD4^{+} T cells from uninfected mice also confirmed our previous observations, revealing clonal expansions with reduced TCR diversity and increase in CD103 expression in most of the clones at day 30 [Figure 4B–F; TCR diversity was assessed by the diversity 50 index (D50), indexes varied from least diverse; 0, to most diverse; 0.5]. However, contrary to expectations for T cell responses to pathogens, newly recruited (Tomato^{+}) IE CD4^{+} T cells from AdV-infected mice, regardless of Ly6A expression, did not show reduced TCR diversity and higher clonal expansions. Instead, CD4^{+} T cells from AdV-infected mice displayed similar or even less clonal expansion than control mice and the Ly6A^{-} population showed significantly higher diversity at day 10 post-infection (Figure 4C–F). Furthermore, recruited CD4^{+}Tomato^{+} T cells in AdV-infected mice displayed limited IEL differentiation, as assessed by CD8αα and CD103 expression at day 30 post-infection, and remained similarly diverse (Figure 4B and Figure S4A).

To initially investigate possible anti-viral functions of gut recruited CD4^{+} T cells, we first assessed a role for TCR expression by these cells. In a recent study, we found that intraepithelial CD4^{+} T cells require TCR expression during their differentiation from peripheral precursors, but not necessarily for maintenance of their epithelial program, or function in a model of bacterial infection (Bilate *et al.*, 2020). We infected mice in which we inducibly deleted TCRα in CD4^{+} T cells (*Cd4*^{CreER}x*Trac*$^{fl/fl}$, iCD4$^{\Delta TCR\alpha}$) immediately

before AdV-infection. We found increased AdV titers in the stool of iCD4$^{\Delta TCR\alpha}$ mice, pointing to a role for the TCR in CD4$^+$ T cell control of viral replication in the intestine (Figure 4G). However, analogous to findings obtained in our previous study (Bilate *et al.*, 2020), excising TCRα from CD4$^+$ T cells 6 days post infection did not impact anti-viral mechanisms during primary, or memory responses (Figure S4B, C). Hence, recruited IE CD4$^+$ T cells post AdV infection retained clonal diversity and the activation marker Ly6A with limited expression of CD103. In contrast, recruited CD4$^+$ T cells in uninfected mice, had reduced clonal diversity and increased CD103 expression over time. Furthermore, our data suggest that TCR signaling is required during CD4$^+$ T cell activation but removal of the TCR post infection does not impact anti-viral mechanisms.

AdV- and CR6-recruited IE CD4$^+$ T cells clear viruses in intestinal organoid cultures

To further examine the ability of virus-recruited CD4$^+$ T cells to regulate viral replication, we developed an intestinal organoid (Sato et al., 2009) and T cell co-culture system *in vitro*. To visualize ongoing AdV infection and replication in the organoids, we used a replication competent mouse adenovirus-2 encoding green fluorescent protein (GFP) fused to the minor capsid protein XI (AdV-GFP) (Wilson *et al.*, 2017). AdV-GFP-infected organoids displayed GFP signal as early as 6 hours post-infection; when cultures were continuously monitored for up to 48 hours (Figure 5A, B and Suppl. Movie 1). We sorted CD4$^+$Tomato$^+$ IE T cells isolated from tamoxifen-treated iSell^{Tomato} mice infected with AdV, CR6 or T1L, 10 days post infection and co-cultured them with AdV-GFP infected organoids (Figure 5C). CD4$^+$Tomato$^+$ IE T cells isolated from either AdV- or CR6-infected mice, but not cells isolated from T1L-infected mice, controlled AdV-GFP replication in intestinal organoids, suggesting that the differentiation of CCR9$^+$Ly6A$^+$CD4$^+$ T cells is associated with cross-protection against enteric viruses (Figure 5D, E and Figure S4D), data that indirectly reinforces the observations that continuous TCR expression by virus-recruited CD4$^+$ T cells may not be required to regulate viral replication. To independently examine the role of TCR engagement in our organoid model, we co-cultured CD4$^+$Tomato$^+$ IE T cells from AdV- and CR6-infected mice with organoids generated from mice deleted of major histocompatibility complex II (MHCII). Consistent with a TCR-independent function, both AdV- and CR6-derived CD4$^+$ T cells controlled AdV-GFP replication in MHCII-deficient organoid cultures (Figure S4E). To specifically address a functional role by recruited Tomato$^+$CD4$^+$ T cells in controlling AdV replication, we sorted Tomato$^+$CCR9$^+$Ly6A$^+$, Tomato$^+$CCR9$^-$Ly6A$^-$, Tomato$^-$CCR9$^+$Ly6A$^+$ and Tomato$^-$CCR9$^-$Ly6A$^-$ IE CD4$^+$ T cells from tamoxifen-treated iSell^{Tomato} mice infected with AdV 10 days post infection and co-cultured them with AdV-GFP infected organoids. We found that Tomato$^+$CCR9$^+$Ly6A$^+$CD4$^+$ T cells had significantly higher capacity for controlling viral replication in the organoids in comparison to other T cell populations (Figure 5F).

We have previously correlated changes in T cell motility with anti-pathogen responses by IELs and detected preferential displacement of IELs to regions containing pathogens using live intravital microscopy (Hoytema van Konijnenburg *et al.*, 2017). Longitudinal imaging analysis of the organoid and T cell co-cultures showed cellular interactions between CD4$^+$ IE T cells derived from AdV infected mice with AdV-infected epithelial cells (Figure 6A).

Tracking of CD4^{+}Tomato^{+} IE T cells from AdV- or CR6-infected mice suggested preferential migration of T cells towards the organoids, which contrasted with CD4^{+} T cells isolated from T1L-infected mice (Figure 6B, C and Suppl. Movies 2–4). Moreover, quantifying cellular velocity revealed that CD4^{+}Tomato^{+} T cells, derived from AdV- or CR6-infected mice, interacting (<20 μm distance) with GFP^{+} epithelial cells slowed down in comparison to non-interacting T cells (>20 μm distance) from the same mice, an occurrence not observed in CD4^{+}Tomato^{+} IE T cells derived from T1L-infected mice (Figure 6D). Therefore, the observed cross-protection by CD4^{+}Tomato^{+} IE T cells derived from AdV- or CR6-infected mice correlates with distinct behavior and proximity to AdV-infected epithelial cells.

ThPOK-dependent CCR9^{+}Ly6A^{+}CD4^{+} IE T cells cross-protect against an enteric virus

Upon arrival to the intestinal epithelium, peripheral CD4^{+} T cells gradually lose the helper T cell lineage-defining transcription factor ThPOK while upregulating the CD8 T cell lineage-defining transcription factor Runt-Related Transcription Factor 3 (Runx3), and T-bet (London *et al.*, 2021; Mucida et al., 2013; Reis *et al.*, 2013; Sujino *et al.*, 2016). This transition is accompanied by the loss of hallmarks associated with T helper subsets, including RORγt or FOXP3 expression, and acquisition of IEL markers including CD244 and CD8αα homodimers (Mucida *et al.*, 2013; Reis *et al.*, 2013). Of note, while we had observed upregulation of granzyme B and IFN-γ by recruited CD4^{+} T cells during viral infection, which are characteristics of IEL differentiation, these cells do not display ThPOK downregulation or express CD8αα (see Figure 1G and Figure S4A above). To determine the role of transcription factors associated with IEL differentiation or CD4 T cell identity in the function and differentiation of gut-recruited CD4 T cells during enteric virus infection, we inducibly and specifically targeted *Zbtb7b* (iCD4$^{\Delta ThPOK}$), *Tbx21* (iCD4$^{\Delta Tbet}$) or *Runx3* (iCD4$^{\Delta Runx3}$) (Mucida *et al.*, 2013; Reis *et al.*, 2014; Reis *et al.*, 2013) in CD4^{+} T cells upon tamoxifen administration prior to infection. AdV-infected iCD4$^{\Delta ThPOK}$ mice displayed significantly reduced viral clearance compared to wild-type (WT) infected controls (Figure 7A), while iCD4$^{\Delta Runx3}$ mice presented delayed clearance but similar control by day 21 post-infection (Figure 7B). iCD4$^{\Delta Tbet}$ showed no differences in viral clearance, compared to WT controls (Figure 7C). Consistent with a functional role for CCR9^{+}Ly6A^{+}CD4^{+} T cells in viral control, AdV-infected iCD4$^{\Delta ThPOK}$ mice did not show recruitment of these cells to the IE and LP compartment 10 days post infection, while iCD4$^{\Delta Tbet}$ and iCD4$^{\Delta Runx3}$ mice displayed significant accumulation similar to control mice (Figure 7D and S5A). Furthermore, CCR9^{+}Ly6A^{+}CD4^{+} IE T cells from AdV-infected iCD4$^{\Delta Runx3}$ and iCD4$^{\Delta ThPOK}$ mice showed reduced IFN-γ production when compared to infected control or iCD4$^{\Delta Tbet}$ mice (Figure 7E and S5B), suggesting that unlike typical Th1 cells, CCR9^{+}Ly6A^{+}CD4^{+} T cell IFN-γ production is Tbet-independent.

To determine if the enhanced IFN-γ production we observed by virus-recruited CD4^{+} T cells mediates the control of AdV infection, we added neutralizing anti-IFN-γ antibodies in the co-culture organoid system. CD4^{+}Tomato^{+} IE T cells were sorted from AdV-infected iSell^{Tomato} mice 10 days post infection and co-cultured with AdV-GFP infected organoids with or without of anti-IFN-γ. Sorted Tomato^{+} T cells inhibited viral replication in the control condition, but not in the presence of neutralizing anti-IFN-γ, indicating that IFN-γ

derived from virus-recruited CD4$^+$ T cells exerts an important function in controlling AdV replication (Figure 7F). Intraepithelial CD4$^+$Tomato$^+$ T cells isolated from CR6-infected mice controlled AdV replication in a similar fashion (Figure S5C and S5D). Conversely, exogenous IFN-γ added to AdV-infected WT organoids readily suppressed virus replication, an effect not observed in *Ifngr1*$^{-/-}$ organoids (Figure S5E). In the same line, we observed impaired viral clearance upon coculturing of IE CD4$^+$Tomato$^+$ T cells from AdV-infected mice with *Ifngr1*$^{-/-}$ organoids (Figure S5F). Finally, *in vivo* treatment of AdV-infected mice with blocking anti-IFNγ antibodies significantly reduced viral clearance (Figure 7G).

Previous studies reported that a combination of the cytokine IL-18 with IL-12 or IL-15 can synergistically augment IFN-γ production by T cells, potentially without TCR stimulation (Tominaga et al., 2000; Yoshimoto et al., 1998). We observed increased *Il12rb2* and *Il15ra* transcripts, but not *Il2rb* or *Il18r1*, by AdV-recruited IE and LP CD4$^+$ T cells (Figure S5G). However, recruited IE and LP CD4$^+$ Tomato$^+$ T cells showed increased IL-18R protein expression in AdV-infected 10 and 30 days post infection compared to CD4$^+$Tomato$^+$ T cells recruited during steady state (Figure S5H), paralleling a preferential expression of IL-18R by CD103$^-$CD4$^+$ IELs when compared to CD103$^+$ CD4$^+$ IELs at steady state, suggesting that CD4 IEL differentiation follows a diverging pathway from IL-18R signaling (Figure S5I). Therefore, we investigated whether these cells produce IFN-γ upon IL-18 stimulation independently of TCR engagement. Sorted intraepithelial CD4$^+$Tomato$^+$ T cells from AdV-infected iSell^{Tomato} mice were stimulated *ex vivo* with IL-12 and/or IL-15 in the presence, or not, of IL-18. While IL-18 stimulation alone induced a modest IFN-γ secretion by CD4$^+$Tomato$^+$ IE T cells, this effect was significantly enhanced upon combination with IL-12 (Figure 7H). After confirming that intestinal organoids produce IL-18 (Figure S5J), we assessed whether IL-18 is necessary for T cell-mediated viral clearance in co-cultures of sorted IE CD4$^+$ Tomato$^+$ from AdV-infected iSell^{Tomato} mice and AdV-GFP infected organoids in the presence, or not, of blocking anti-IL-18 antibodies. While sorted IE CD4$^+$ Tomato$^+$ T cells efficiently inhibited viral replication, IL-18 blockage reversed this effect (Figure 7I). Moreover, *in vivo* treatment of AdV-infected mice with blocking anti-IL-18 antibodies also significantly reduced viral clearance (Figure S5K).

Finally, we addressed whether the cross-protective activity observed for CR6-recruited CD4$^+$ IE T cells in the AdV-infected organoid system could be recapitulated *in vivo*. Tamoxifen-treated iCD4$^{\Delta ThPOK}$ or wild-type control mice were infected with CR6 or vehicle, and 10 days later, infected with AdV. WT mice infected with CR6 prior to AdV-infection displayed accelerated AdV clearance compared to vehicle-treated mice, reinforcing the possibility of cross-protection. This phenomenon was dependent on ThPOK expression by CD4$^+$ T cells as tamoxifen-treated CR6-infected iCD4$^{\Delta ThPOK}$ mice did not show reduction in stool AdV titers post infection (Figure 7J). Additionally, as observed during primary AdV infection, initial engagement of the TCR on CD4$^+$ T cells during the primary CR6-infection was also necessary for cross-protection against AdV, as CR6-infected iCD4$^{\Delta TCR\alpha}$ mice displayed increased AdV titers in the stool when compared to wild-type control mice (Figure 7K). Furthermore, excising TCRα from CD4$^+$ T cells 6 days post CR6-infection did not impact cross-protection by the recruited CD4$^+$ T cells against AdV infection (Figure S5L). Hence, ThPOK-dependent CCR9$^+$Ly6A$^+$CD4$^+$ T cells induced by

AdV or CR6 are recruited to the IE compartment, acquiring an increased IFN-γ production that controls AdV viral replication *in vivo* and *in vitro*.

Discussion

By developing a mouse genetic strategy allowing for the fate-mapping of newly recruited polyclonal T cells to the intestinal tissue, our study uncovered an important role of $CD4^+$ IELs in the protection against enteric adenovirus infection. The fate-mapping approach also revealed that while MNV (CR6) and AdV, viruses with tropism for the epithelium, induced a robust $CD4^+$ T cell recruitment to the epithelium, CW3 and Reovirus T1L, viruses that predominantly infect cells in the LP, preferentially recruited CD8αβ T cells to both LP and IE compartments. After initial priming in the gut-draining LNs (Esterhazy et al., 2019), newly recruited T cells are further exposed to gut tissue signals in the LP, a site with much higher density of myeloid cell populations than the intestinal epithelium (London *et al.*, 2021). This stepwise process probably plays an important role in the differentiation of $CCR9^+Ly6A^+CD4^+$ T cells, which are exposed to TCR- and cytokine-signals, including IL-12 and IL-18, before even reaching the epithelium. Such intra-tissue specialization, directly associated with the site of insult, highlights distinct lymphocyte differentiation strategies, as recently demonstrated during steady state (London *et al.*, 2021) and infection (Kiner *et al.*, 2021). Nonetheless, whether newly recruited LP *versus* IE $CD4^+$ T cells play complementary or redundant roles during infections remains to be determined.

Upon arriving in the IE compartment at steady state, recruited peripheral $CD103^-$ $CD4^+$ T cells gradually acquire an IEL phenotype, progressively acquiring CD103 and CD8αα expression (Bilate *et al.*, 2020; London *et al.*, 2021). During this process, a progressive loss of ThPOK allows for increased imprinting by other transcription factors including Runx3 and T-bet, resulting in acquisition of a cytotoxic machinery (London *et al.*, 2021; Mucida *et al.*, 2013; Reis *et al.*, 2014; Reis *et al.*, 2013). As virus-induced cytotoxic $CD4^+$ effector T cells have previously been identified in several murine models (Brien et al., 2008; Hou et al., 1992; Stuller et al., 2010) as well as human viral infections (Swain et al., 2012; van Leeuwen et al., 2004; Zaunders et al., 2004). IEL differentiation would presumably facilitate response to viruses (Mucida *et al.*, 2013; Reis *et al.*, 2013). While we observed preferential epithelial recruitment of $CD4^+$ T cells in the context of AdV or chronic MVN infections, acquisition of an CTL-like IEL program was prevented and $CD4^+$ T cells instead differentiated into IFN-γ-producing $CCR9^+Ly6A^+$ cells functionally dependent on continuous ThPOK expression. ThPOK has been previously shown to modulate Th1 phenotype during effector differentiation (Vacchio et al., 2014). Additionally, a role for ThPOK in the “functional fitness” of $CD4^+$ T cells during responses to systemic LCMV was recently reported (Ciucci et al., 2019), supporting a role for this transcription factor in anti-viral CD4 T cell responses.

In contrast to the IEL differentiation pathway (London *et al.*, 2021), we observed that AdV-recruited IE $CD4^+$ T cells acquired a mixed Th1 and CTL effector phenotype with most of the cells expressing CD69, resembling some characteristics associated to tissue resident memory (T_{RM}) though lacking CD103 expression (Mackay et al., 2013; Masopust and Soerens, 2019). Furthermore, a recent study reported that $CD103^-$ T_{RM} had

increased proliferative potential and enhanced function but could also readily modulate their phenotype upon relocation, in contrast to CD103$^+$ T_{RM} (Christo et al., 2021). The distinct differentiation of the fate-mapped cells suggests that the lack of CD103 expression and IEL differentiation is due to a cell-intrinsic regulation. It is possible that their TGF-β signaling is impaired (Konkel et al., 2011; Reis *et al.*, 2013) or that pathways upregulated by these cells counteract Runx3-mediated IEL differentiation. Runx3, which has been previously associated with CTL (Lotem et al., 2013), IEL (Reis *et al.*, 2013) and T_{RM} (Milner et al., 2017) differentiation, is not required for upregulation of CCR9 or Ly6A by virus-recruited CD4$^+$ T cells, but regulates IFN-γ production by these cells. Our data overall suggest a major role for IFN-γ, rather than CTL activity, in the anti-viral activity of these cells. Hence, although the differentiation of IE-recruited CD4$^+$ T cells upon virus infection appears to follow a distinct path from T_{RM} and IEL CD4$^+$ T cells, it could be related to CTL CD4$^+$ T cell responses observed in other tissues, a possibility that requires additional investigation supported by our observations reported here.

Another characteristic of peripheral T cell recruitment to the IE compartment is clonal expansion and progressive loss of TCR diversity as they undergo IEL differentiation during homeostasis (Bilate *et al.*, 2020). In contrast to these steady state observations, virus-recruited IE CD4$^+$ T cells displayed a clonally diverse TCR population, which is comparable to what has been described for peripheral CD4$^+$ T cells upon LCMV infection (Khatun et al., 2021). Nevertheless, corresponding to our observations under steady state (Bilate *et al.*, 2020), while TCR expression was required for initial differentiation and function of IE-recruited CD4$^+$ IELs, TCR removal post infection did not impact the capacity of virus-recruited CD4$^+$ T cells to control viral replication. This observation, in addition to reinforcing the notion that IE T cells may depend less on TCR engagement to exert their function than peripheral T cells (Bilate *et al.*, 2020), may explain their ability to cross protect against unrelated viruses *in vivo* and in our organoid model. The capacity of recruited CD4$^+$ T cells to secrete IFN-γ in response to IL-18 in combination to IL-12 or IL-15, independent of TCR engagement, is similar to what has been described to memory CD8$^+$ T cells (Ariotti et al., 2014) and could represent a general mechanism co-opted by IELs to confer broad protection in the epithelium. Conversely, cross-protection to unrelated pathogens has been previously reported to skin-resident CD8αβ$^+$ T cells upon herpes simplex virus infection (Ariotti *et al.*, 2014).

A relevant point in our studies is that functional IE-recruited CD4$^+$ IELs were primarily found in a chronic viral model, raising the possibility that targeting strategies to enhance the function of this population may benefit viral control. Primary or secondary (cross-protection) viral clearance data indicated the functional relevance of transcription factors associated with the development of CCR9$^+$Ly6A$^+$CD4$^+$ T cells, or their capacity to secrete IFN-γ, observations related to previous reports describing a crucial role for this cytokine in the human adenovirus replication (Mistchenko et al., 1989). Additionally, germ-free mice display reduced numbers of IFN-γ-producing CD4$^+$ T cells the intestine, a phenotype that can be rescued by MNV-CR6 infection (Kernbauer et al., 2014). Our study indicates that enteric viral infections promote distinct T cell responses with intra-tissue specialization within the intestine, with previously unappreciated characteristics of TCR repertoire and requirements, surface markers and functional adaptation.

Limitations of the study

Our study primarily focused on understanding the functional role of intestinal $CD4^+$ T cells during murine adenovirus-2 infection. While our data indicate that MNV-CR6 induced $CCR9^+Ly6A^+CD4^+$ T cells cross-protect against AdV-infection, we have not addressed the opposite as MNV-CR6 is known to induce a lifelong chronic infection that cannot be cleared by cell mediated or humoral adaptive immunity (Nice et al., 2015). Because our data suggests that $CD4^+$ T cells recruited by *L. monocytogenes*, share similarities virus-recruited T cells, yet do not upregulate CCR9, future studies are needed to determine whether additional pathogens can trigger analogous TCR-independent T cell effector function. Further investigation is also needed to determine if similar mechanisms described in this study occur during infection with other enteric viruses. Moreover, follow up studies should address whether similar pathways exist beyond the intestine and if this information can be translated to human virus infections.

STAR Methods

RESOURCE AVAILABILITY

Lead Contact—Further information and requests for resources and reagents should be directed to and will be fulfilled by the Lead Contact, Daniel Mucida (mucida@rockefeller.edu).

Materials Availability—All animal strains used in this study are available from The Jackson Laboratory or were provided by the indicated investigators. All mice are available upon request, but due to the complexity of the crosses, availability may be limited. This study did not generate any new unique reagents.

Data and Code Availability

- The raw IE and LP T cell RNA sequencing data, IE TCR sequencing data and processed files reported in this study have been deposited in GEO and are publicly available as of the date of publication. The accession number is listed in the key resources table.
- This paper does not report original code.
- Any additional information required to reanalyze the data reported in this paper is available from the lead contact upon request.

EXPERIMENTAL MODEL AND SUBJECT DETAILS

Animals—Animal care and experimentation were consistent with NIH guidelines and were approved by the Institutional Animal Care and Use Committee at the Rockefeller University. B6.129S2-H2$^{dlAb1\text{-}Ea}$/J (Jax: 003584), *Rosa26*$^{CAG\text{-}LSL\text{-}tdTomato\text{-}WPRE}$ (007914), *Zbtb7b*$^{fl/fl}$ (009369), *Cd4*$^{Cre\text{-}ERT2}$ (022356), *Ifngr1*$^{-/-}$ (003288) and *Tbx21*$^{fl/fl}$ (022741) mice were purchased from Jackson Laboratories and housed in our facility. *Trac*$^{f/f}$ mice were kindly provided by A. Rudensky (MSKCC). *Runx3*$^{fl/fl}$ (008773) mice were provided by T. Egawa (Washington University in St. Louis). *Sell*$^{Cre\text{-}ERT2}$ mice were provided by M. Nussenzweig (Merkenschlager *et al.*, 2021). Several of these lines were interbred in our facilities to obtain

the final strains described elsewhere in the text. Genotyping was performed according to the protocols established for the respective strains by Jackson Laboratories or by donor investigators. Mice were maintained at the Rockefeller University animal facility under specific pathogen-free (SPF) conditions. Both male and female littermates were used, age 7–12 weeks old.

Oral infection with *Listeria monocytogenes*—*L. monocytogenes* 10403S-inlA strain expressing full-length OVA (Lm-OVA) were grown overnight in brain heart infusion media. Lm-OVA was provided by L. Lefrançois. Mice were infected with 10^9 colony forming units (CFU) 24h after oral treatment with 20 mg of Streptomycin (Sigma-Aldrich) diluted in water. At day 9 post-infection, intraepithelial lymphocytes were harvested and stained with MHCII-restricted LLO-tetramer (NIH) and analyzed by flow cytometry.

METHOD DETAILS

Oral infection with viruses—WT mouse adenovirus-2(AdV) and AdV-GFP [previously called “MAdV-2.IXeGFP (Wilson *et al.*, 2017)] were propagated in the mouse rectal carcinoma CMT-93 cell line (ATCC CCL-223), purified, and quantified as previously described (Gounder et al., 2016). Mice were infected with 10^7 infectious units of WT AdV in 100 ul PBS by oral gavage. Reovirus T1L (T1L) was provided by T. Dermody (University of Pittsburgh) and propagated in L929 cell line, purified and quantified as previously described (Kobayashi et al., 2010). T1L. Mice were infected with 10^8 plaque forming units (pfu) of T1L in 100 ul PBS by oral gavage. Murine norovirus (MVN) CW3 and CR6 were provided by K. Cadwell (New York University) and was propagated in RAW264.7 cell line, purified and quantified as previously described (Kernbauer *et al.*, 2014). Mice were infected with 3×10^6 pfu of MNV CW3 or CR6 in 100 ul PBS by oral gavage.

Tamoxifen Treatment—Tamoxifen (Sigma) was dissolved in corn oil (Sigma) and 10% ethanol, shaking at 37°C for 30 min-1 h. Two doses of Tamoxifen (5 mg/dose) were administered to mice via oral gavage at 50 mg/mL, 3 days and 1 day before viral infection.

Adenovirus fecal shedding—1 or 2 stool pellets were collected at the days post infection as indicated in the figure legends and frozen at −80°C. On the day of processing, stool samples were weighed and processed with QIAamp Fast DNA Stool Mini Kit (Qiagen) for DNA extraction following the manufacturer’s instructions. Samples were measured for DNA content by NanoDrop (Thermo Scientific). RT-qPCR was performed using PowerSYBR Green (Applied Biosystems) with AdV specific primers; FW: 5’-GTCCGATTCGGTACTACGGT-3’; RV: 5’-GTCAGACAACTTCCCAGGGT-3’, at an annealing temperate of 55°C and for 40 cycles on a QuantStudio 3 RT PCR System (Applied Biosystems). Genomic copies were determined by correlation to an AdV DNA standard and normalized to DNA input and stool weight. Stool from uninfected mice was used as a negative control.

Isolation of intestinal T cells—Small intestine intraepithelial and lamina propria lymphocytes were isolated as previously described (Reis *et al.*, 2013). Briefly, small intestines were harvested and washed in PBS and 1 mM dithiothreitol (DTT) followed by

30 mM EDTA. Intraepithelial cells were recovered from the supernatant of DTT and EDTA washes. Lymphocytes from lamina propria were obtained after collagenase digestion of the tissue. Mononuclear cells were isolated by gradient centrifugation using Percoll. Single-cell suspensions were then stained with fluorescently labeled antibodies for 25 min at 4° C prior to downstream flow cytometry (analysis or sorting) as specified in figure legends.

Staining Strategy—The following gating strategy was utilized to examine $CD4^+$ T cells: single live lymphocytes (based on size and live/dead fixable dye Aqua stain), $CD45^+$, $TCR\gamma\delta^-$, $TCR\beta^+$, $CD8\beta^{low/-}$, $CD4^+$. For analysis of $iSell^{Tomato}$, the following gating strategy was added: $CD62L^-$ and $Tomato^+$. For single-cell sorting of cells subjected to scTCRseq the following gating strategy was used: single live lymphocytes, CD45+, $TCR\gamma\delta^-$, $TCR\beta^+$, $CD4^+$, $CD62L^-$, $Tomato^+$, $Ly6a^{+/-}$, $CD103^{+/-}$, $CD8\alpha^{+/-}$. For sorting of cells subjected to bulk RNaseq we used single live lymphocytes $CD45^+$, $TCR\gamma\delta^-$, $TCR\beta^+$, $CD8\beta^-$, $CD4^+$, $Tomato^+$ and $CD62L^-$. For sorting of T cells subjected to organoid co-cultures, we gated on single live lymphocytes $CD45^+$ $TCR\gamma\delta^-$, $CD8\beta^-$, $CD62L^-$, $MHCII^-$, $CD11b^-$, $CD11c^-$, $CD19^-$, $NK1.1^-$, $Tomato^+$ and $CD5^+$.

***In vivo* IFN-γ or IL-18 blocking—**Mice were injected with 500 μg of anti-IFN-γ (XMG1.2, BioXCell) or Rat IgG1 (HRPN, BioXCell) intraperitoneally at day 8, 10, 12, 14, 16 and 18 post infection. Mice were injected with 100 μg of anti-IL-18 (YIGIF74–1G7, BioxCell) or Rat IgG2a (2A3, BioxCell) intraperitoneally at day 9, 10, 11, 12 and 13 post infection.

***In vitro* T cell cultures—**$iSell^{Tomato}$ mice were infected with AdV and $CD45^+CD62L^-CD4^+Tomato^+$ IE T cells were sorted 10 days post infection. Sorted T cells were cultured in RPMI 1640 (Gibco), 10% FBS (Sigma), 1% Pen/Strep (Gibco), 1% L-glutamine (Gibco), 1% Sodium Pyruvate (Gibco), 2% Non-essential Amino Acids (Gibco), 2.5% 1M HEPES (Gibco), 50μM 2-Mercaptoethanol (Sigma), 10 ng/ml recombinant murine IL-2 (R&D) and 5 ng/ml recombinant murine IL-7 (R&D) at 10–20.000 cells/well in a 96-well round bottom plate (Corning). T cells were stimulated with 10 ng/ml recombinant murine IL-12 (R&D), 10 ng/ml recombinant murine IL-15/IL-15Rα complex (ThermoFisher) and 10 ng/ml recombinant murine IL-18 (R&D). Supernatants were collected 24-hour post stimulation and IFN-γ was measured with IFN-γ ELISA (Invitrogen) by following manufacturer's instructions.

Intracellular Staining and Flow Cytometry—For analysis of cytokine secretion, total mononuclear cells isolated from the epithelium were plated in 48-well plates and incubated at 37° C with 100 ng/mL phorbol 12-myristate 13-acetate (PMA, Sigma), 200 ng/mL ionomycin (Sigma) and 2mM monensin (BD Biosciences) for 4 hours. Intracellular staining for IFN-γ and granzyme B was conducted in Perm/Wash buffer after fixation and permeabilization in Fix/Perm buffer (BD Biosciences, USA) according to kit instructions. Flow cytometry data were acquired on an LSR-II flow cytometer (Becton Dickinson,USA) and analyzed using FlowJo 10 software package (Tri-Star, USA).

Organoids and co-cultures—Organoids were established from crypts isolated from adult mouse small intestine and maintained as described previously (Rogoz et al., 2015; Sato

et al., 2009). For infection and co-cultures, organoids were removed from the Matrigel by gently pipet off the top media layer and 500 µl of cold culture media containing 10% FBS (Sigma F0926) was added to each well to dissolve the Matrigel. Organoids was washed with cold culture media containing 10% FBS and 30–40 organoids were infected with 10^4 i.u. of AdV-GFP in 500 µl cold PBS for 20 min on ice. Inoculum was discarded and infected organoids was washed with 15 ml of T-cell culture medium (TCM) [RPMI 1640, 10% FBS, 1% Pen/Strep (Gibco), 1% L-glutamine (Gibco), 1% Sodium Pyruvate (Gibco), 2% Non-essential Amino Acids (Gibco), 2.5% 1M HEPES (Gibco), 50µM 2-Mercaptoethanol (Sigma)]. Then, working on ice, 30 µl of 2–3×10^4 sorted $CD4^+Tomato^+$ T cells in TCM was carefully added to 30 ul of 8–12 infected organoids in 30 µl TCM, next we added 40 ul of ice cold Matrigel. 100 µl of the T cell/organoid/Matrigel mixture was immediately added to a preheated (37°C) 96-well culture plate with glass bottoms (MatTek). The culture plate was incubated for 20–30 min in 37°C to let the Matrigel polymerize. Next, we added 200 µl of TCM containing 50 ng/ml recombinant murine EGF, 100 ng/ml recombinant murine Noggin, 500 ng/ml recombinant human R-spondin, 10 ng/ml recombinant murine IL-2 (R&D), 5 ng/ml recombinant murine IL-7 (R&D) and 10 ng/ml recombinant murine IL-15/IL-15Rα complex (ThermoFisher) on top of the polymerized Matrigel. For IFN-γ neutralizing experiments, we added 10 µg/ml of anti-IFN-γ (XMG1.2, BD Biosciences). For IFN-γ stimulation, we added 10 ng/ml of IFN-γ (R&D). For IL-18 neutralizing experiments, we added 50 µg/ml of anti-IL-18 (YIGIF74–1G7, BioXcell)

Organoid analysis and T cell tracking—Live imaging was performed on the CellVoyager (Yokagawa/Olympus) spinning disk confocal microscope at 37°C and with 5% CO_2. Co-cultures were imaged in 96-well plates with glass bottoms (MatTek). 10 to 12 z-stacks of 1.52 µm step-size were acquired every 6–7 min for 48 hours. GFP signal above background per organoid was used to measure the GFP expression area for each z-stack and time point. Organoid area was determined with brightfield images for each z-stack and time point and used to normalize the GFP expression area for each respective z-stack and time point. For T cell tracking, hyperstacks were made of each z-stack, time point and channel. T cell ($Tomato^+$) and infected epithelial (GFP^+) tracking was obtained with TrackMate 6.0.2 (Tinevez et al., 2017) on hyperstacked images and over time, cell diameter was set at 14 µm to obtain optimal tracking. $Tomato^+$ T cell tracking 3D coordinates was analyzed together with GFP^+ infected epithelial 3D coordinates. If a $Tomato^+$ track point was within 20µm radius of a GFP^+ track point in any dimension at a specific given time, that track point was considered as an interacting point. A minimum of 8 sequential interacting points in a specific T cell track were used to calculate the cell average velocity. Reconstruction of images were done using a Python script and the skimage v.0.19 package. Image quantifications and modulations were made in ImageJ 2.1 and all image calculations were made in R studio 1.2.5.

Single-Cell TCR Sequencing—Single cells were index-sorted using a FACS Aria into 96-well plates containing 5µL of lysis buffer (TCL buffer, QIAGEN 1031576) supplemented with 1% β-mercaptoethanol) and frozen at −80° C prior to RT-PCR. RNA and RT-PCRs for TCRβ were prepared as previously described (Dash et al., 2011). PCR products for TCRβ were multiplexed with barcodes and submitted for MiSeq sequencing (Han et al., 2014)

using True Seq Nano kit (Illumina). Fastq files were de-multiplexed and paired-end reads were assembled at their overlapping region using the PANDASEQ (Masella et al., 2012) and FASTAX toolkit. Demultiplexed and collapsed reads were assigned to wells according to barcodes. Fasta files from MiSeq sequences were then aligned and analyzed on IMGT (http://imgt.org/HighV-QUEST) (Brochet et al., 2008). Cells with identical TCRβ CDR3 nucleotide sequences were considered as the same clones.

Bulk RNA-seq Library Preparation—Sorted cells (800 cells) were lysed in a guanidine thiocyanate buffer (TCL buffer, QIAGEN) supplemented with 1% β-mercaptoethanol. RNA was isolated by solid-phase reversible immobilization bead cleanup using RNAClean XP beads (Agentcourt, A63987), reversibly transcribed, and amplified as described (Trombetta et al., 2014). Uniquely barcoded libraries were prepared using the Nextera XT kit (Illumina) following the manufacturer's instructions. Sequencing was performed on an Illumina NextSeq500 for a total yield of 400M reads.

Bulk RNA-seq Analysis—Raw fastq files were processed by using the mouse transcriptome (gencode M23) with the kallisto (v0.46) software (Bray et al., 2016). Analysis of transcript quantification was performed at the gene level by using the sleuth (v0.30) package for R (Pimentel et al., 2017). In short, we modeled batch effect and our experimental design using the sleuth_fit function and detected differentially expressed genes between all groups by the likelihood ratio test (LRT). To determine significantly expressed genes between group pairs, we used the wald-test function. All downstream analysis was made using genes below adjusted p value of 0.05. TCRα and TCRβ CDR3 sequences were reconstructed *in silico* using MixCR software (Bolotin et al., 2015) and the extracted sequences were analyzed with the Immunarch package (v0.6.5) for R (10.5281/zenodo.3893991).

QUANTIFICATION AND STATISTICAL ANALYSIS

Statistical Analyses—Statistical analysis was carried out using GraphPad Prism v.9. Flow cytometry analysis was carried out using FlowJo software. Data in graphs show mean and p values < 0.05 were considered significant. Repertoire diversity was analyzed by the Diversity 50 (D50). Diversity 50 (D50) was calculated using Excel version 16 as the fraction of dominant clones that account for the cumulative 50% of the TCRβ CDR3s identified. GraphPadPrism v.9 was used for graphs and Adobe Illustrator 2020 used to assemble and edit figures.

Supplementary Material

Refer to Web version on PubMed Central for supplementary material.

Acknowledgments

We are grateful to A. Rogoz, H. Lugo and S. Gonzalez for exceptional animal care, mouse colony management and genotyping; Yasmeen Khan, the Genomics Core, the Bio-Imaging Resource Center (RRID:SCR_017791), and additional Rockefeller University employees for continuous assistance. We thank the NIH tetramer facility for providing the LLO tetramer. We thank A. Bilate for providing advice on the TCR sequencing and editing the manuscript, A. Lockhart for editing the manuscript and all the members of the Mucida, Victora (Rockefeller) and Lafaille (NYU) labs for fruitful discussions. Graphical abstract was created with BioRender.com.

This work was supported by the Black Family Metastasis Center, the Burroughs Wellcome Fund PATH Award, the Mathers Foundation, the Pershing Square Foundation, the FASI/FARE Consortium and National Institute of Health grants R21AI144827, R01DK113375 and R01DK093674, and the Howard Hughes Medical Institute (D.M.). R.P. was supported by the Swedish Research Council and The Sweden-America Foundation.

References

Ariotti S, Hogenbirk MA, Dijkgraaf FE, Visser LL, Hoekstra ME, Song JY, Jacobs H, Haanen JB, and Schumacher TN (2014). T cell memory. Skin-resident memory CD8(+) T cells trigger a state of tissue-wide pathogen alert. Science 346, 101–105. 10.1126/science.1254803. [PubMed: 25278612]

Bilate AM, London M, Castro TBR, Mesin L, Bortolatto J, Kongthong S, Harnagel A, Victora GD, and Mucida D (2020). T Cell Receptor Is Required for Differentiation, but Not Maintenance, of Intestinal CD4(+) Intraepithelial Lymphocytes. Immunity 53, 1001–1014 e1020. 10.1016/j.immuni.2020.09.003. [PubMed: 33022229]

Bolotin DA, Poslavsky S, Mitrophanov I, Shugay M, Mamedov IZ, Putintseva EV, and Chudakov DM (2015). MiXCR: software for comprehensive adaptive immunity profiling. Nature methods 12, 380–381. 10.1038/nmeth.3364. [PubMed: 25924071]

Bouziat R, Hinterleitner R, Brown JJ, Stencel-Baerenwald JE, Ikizler M, Mayassi T, Meisel M, Kim SM, Discepolo V, Pruijssers AJ, et al. (2017). Reovirus infection triggers inflammatory responses to dietary antigens and development of celiac disease. Science 356, 44–50. 10.1126/science.aah5298. [PubMed: 28386004]

Bray NL, Pimentel H, Melsted P, and Pachter L (2016). Near-optimal probabilistic RNA-seq quantification. Nature biotechnology 34, 525–527. 10.1038/nbt.3519.

Brien JD, Uhrlaub JL, and Nikolich-Zugich J (2008). West Nile virus-specific CD4 T cells exhibit direct antiviral cytokine secretion and cytotoxicity and are sufficient for antiviral protection. Journal of immunology 181, 8568–8575. 10.4049/jimmunol.181.12.8568.

Brochet X, Lefranc MP, and Giudicelli V (2008). IMGT/V-QUEST: the highly customized and integrated system for IG and TR standardized V-J and V-D-J sequence analysis. Nucleic acids research 36, W503–508. 10.1093/nar/gkn316. [PubMed: 18503082]

Cervantes-Barragan L, Chai JN, Tianero MD, Di Luccia B, Ahern PP, Merriman J, Cortez VS, Caparon MG, Donia MS, Gilfillan S, et al. (2017). Lactobacillus reuteri induces gut intraepithelial CD4(+)CD8alphaalpha(+) T cells. Science 357, 806–810. 10.1126/science.aah5825. [PubMed: 28775213]

Christo SN, Evrard M, Park SL, Gandolfo LC, Burn TN, Fonseca R, Newman DM, Alexandre YO, Collins N, Zamudio NM, et al. (2021). Discrete tissue microenvironments instruct diversity in resident memory T cell function and plasticity. Nature immunology 22, 1140–1151. 10.1038/s41590-021-01004-1. [PubMed: 34426691]

Ciucci T, Vacchio MS, Gao Y, Tomassoni Ardori F, Candia J, Mehta M, Zhao Y, Tran B, Pepper M, Tessarollo L, et al. (2019). The Emergence and Functional Fitness of Memory CD4(+) T Cells Require the Transcription Factor Thpok. Immunity 50, 91–105.e104. 10.1016/j.immuni.2018.12.019. [PubMed: 30638736]

Dash P, McClaren JL, Oguin TH 3rd, Rothwell W, Todd B, Morris MY, Becksfort J, Reynolds C, Brown SA, Doherty PC, and Thomas PG (2011). Paired analysis of TCRalpha and TCRbeta chains at the single-cell level in mice. The Journal of clinical investigation 121, 288–295. 10.1172/JCI44752. [PubMed: 21135507]

Edelblum KL, Singh G, Odenwald MA, Lingaraju A, El Bissati K, McLeod R, Sperling AI, and Turner JR (2015). gammadelta Intraepithelial Lymphocyte Migration Limits Transepithelial Pathogen Invasion and Systemic Disease in Mice. Gastroenterology 148, 1417–1426. 10.1053/j.gastro.2015.02.053. [PubMed: 25747597]

Esterhazy D, Canesso MCC, Mesin L, Muller PA, de Castro TBR, Lockhart A, ElJalby M, Faria AMC, and Mucida D (2019). Compartmentalized gut lymph node drainage dictates adaptive immune responses. Nature 569, 126–130. 10.1038/s41586-019-1125-3. [PubMed: 30988509]

Faria AMC, Reis BS, and Mucida D (2017). Tissue adaptation: Implications for gut immunity and tolerance. J Exp Med 214, 1211–1226. 10.1084/jem.20162014. [PubMed: 28432200]

Florsheim EB, Sullivan ZA, Khoury-Hanold W, and Medzhitov R (2021). Food allergy as a biological food quality control system. Cell 184, 1440–1454. 10.1016/j.cell.2020.12.007. [PubMed: 33450204]

Gounder AP, Myers ND, Treuting PM, Bromme BA, Wilson SS, Wiens ME, Lu W, Ouellette AJ, Spindler KR, Parks WC, and Smith JG (2016). Defensins Potentiate a Neutralizing Antibody Response to Enteric Viral Infection. PLoS Pathog 12, e1005474. 10.1371/journal.ppat.1005474. [PubMed: 26933888]

Grau KR, Roth AN, Zhu S, Hernandez A, Colliou N, DiVita BB, Philip DT, Riffe C, Giasson B, Wallet SM, et al. (2017). The major targets of acute norovirus infection are immune cells in the gut-associated lymphoid tissue. Nat Microbiol 2, 1586–1591. 10.1038/s41564-017-0057-7. [PubMed: 29109476]

Graziano VR, Alfajaro MM, Schmitz CO, Filler RB, Strine MS, Wei J, Hsieh LL, Baldridge MT, Nice TJ, Lee S, et al. (2021). CD300lf Conditional Knockout Mouse Reveals Strain-Specific Cellular Tropism of Murine Norovirus. J Virol 95. 10.1128/JVI.01652-20.

Han A, Glanville J, Hansmann L, and Davis MM (2014). Linking T-cell receptor sequence to functional phenotype at the single-cell level. Nature biotechnology 32, 684–692. 10.1038/nbt.2938.

Honda K, and Littman DR (2016). The microbiota in adaptive immune homeostasis and disease. Nature 535, 75–84. 10.1038/nature18848. [PubMed: 27383982]

Hou S, Doherty PC, Zijlstra M, Jaenisch R, and Katz JM (1992). Delayed clearance of Sendai virus in mice lacking class I MHC-restricted CD8+ T cells. Journal of immunology 149, 1319–1325.

Hoytema van Konijnenburg DP, Reis BS, Pedicord VA, Farache J, Victora GD, and Mucida D (2017). Intestinal Epithelial and Intraepithelial T Cell Crosstalk Mediates a Dynamic Response to Infection. Cell 171, 783–794 e713. 10.1016/j.cell.2017.08.046. [PubMed: 28942917]

Iliev ID, and Cadwell K (2021). Effects of Intestinal Fungi and Viruses on Immune Responses and Inflammatory Bowel Diseases. Gastroenterology 160, 1050–1066. 10.1053/j.gastro.2020.06.100. [PubMed: 33347881]

Jabri B, and Sollid LM (2009). Tissue-mediated control of immunopathology in coeliac disease. Nature reviews. Immunology 9, 858–870. nri2670 [pii] 10.1038/nri2670.

Kernbauer E, Ding Y, and Cadwell K (2014). An enteric virus can replace the beneficial function of commensal bacteria. Nature 516, 94–98. 10.1038/nature13960. [PubMed: 25409145]

Khatun A, Kasmani MY, Zander R, Schauder DM, Snook JP, Shen J, Wu X, Burns R, Chen YG, Lin CW, et al. (2021). Single-cell lineage mapping of a diverse virus-specific naive CD4 T cell repertoire. J Exp Med 218. 10.1084/jem.20200650.

Kiner E, Willie E, Vijaykumar B, Chowdhary K, Schmutz H, Chandler J, Schnell A, Thakore PI, LeGros G, Mostafavi S, et al. (2021). Gut CD4(+) T cell phenotypes are a continuum molded by microbes, not by TH archetypes. Nature immunology 22, 216–228. 10.1038/s41590-020-00836-7. [PubMed: 33462454]

Kobayashi T, Ooms LS, Ikizler M, Chappell JD, and Dermody TS (2010). An improved reverse genetics system for mammalian orthoreoviruses. Virology 398, 194–200. 10.1016/j.virol.2009.11.037. [PubMed: 20042210]

Konkel JE, Maruyama T, Carpenter AC, Xiong Y, Zamarron BF, Hall BE, Kulkarni AB, Zhang P, Bosselut R, and Chen W (2011). Control of the development of CD8alphaalpha+ intestinal intraepithelial lymphocytes by TGF-beta. Nature immunology 12, 312–319. 10.1038/ni.1997. [PubMed: 21297643]

London M, Bilate AM, Castro TBR, Sujino T, and Mucida D (2021). Stepwise chromatin and transcriptional acquisition of an intraepithelial lymphocyte program. Nature immunology 22, 449–459. 10.1038/s41590-021-00883-8. [PubMed: 33686285]

Lotem J, Levanon D, Negreanu V, Leshkowitz D, Friedlander G, and Groner Y (2013). Runx3-mediated transcriptional program in cytotoxic lymphocytes. PloS one 8, e80467. 10.1371/journal.pone.0080467. [PubMed: 24236182]

Mackay LK, Rahimpour A, Ma JZ, Collins N, Stock AT, Hafon ML, Vega-Ramos J, Lauzurica P, Mueller SN, Stefanovic T, et al. (2013). The developmental pathway for CD103(+)CD8+ tissue-

resident memory T cells of skin. Nature immunology 14, 1294–1301. 10.1038/ni.2744. [PubMed: 24162776]

Masella AP, Bartram AK, Truszkowski JM, Brown DG, and Neufeld JD (2012). PANDAseq: paired-end assembler for illumina sequences. BMC bioinformatics 13, 31. 10.1186/1471-2105-13-31. [PubMed: 22333067]

Masopust D, and Soerens AG (2019). Tissue-Resident T Cells and Other Resident Leukocytes. Annual review of immunology 37, 521–546. 10.1146/annurev-immunol-042617-053214.

McDonald BD, Jabri B, and Bendelac A (2018). Diverse developmental pathways of intestinal intraepithelial lymphocytes. Nature reviews. Immunology 18, 514–525. 10.1038/s41577-018-0013-7.

Merkenschlager J, Finkin S, Ramos V, Kraft J, Cipolla M, Nowosad CR, Hartweger H, Zhang W, Olinares PDB, Gazumyan A, et al. (2021). Dynamic regulation of TFH selection during the germinal centre reaction. Nature 591, 458–463. 10.1038/s41586-021-03187-x. [PubMed: 33536617]

Milner JJ, Toma C, Yu B, Zhang K, Omilusik K, Phan AT, Wang D, Getzler AJ, Nguyen T, Crotty S, et al. (2017). Runx3 programs CD8(+) T cell residency in non-lymphoid tissues and tumours. Nature 552, 253–257. 10.1038/nature24993. [PubMed: 29211713]

Mistchenko AS, Diez RA, and Falcoff R (1989). Inhibitory effect of interferon-gamma on adenovirus replication and late transcription. Biochem Pharmacol 38, 1971–1978. 10.1016/0006-2952(89)90496-6. [PubMed: 2500934]

Mucida D, Husain MM, Muroi S, van Wijk F, Shinnakasu R, Naoe Y, Reis BS, Huang Y, Lambolez F, Docherty M, et al. (2013). Transcriptional reprogramming of mature CD4(+) helper T cells generates distinct MHC class II-restricted cytotoxic T lymphocytes. Nature immunology 14, 281–289. 10.1038/ni.2523. [PubMed: 23334788]

Nice TJ, Baldridge MT, McCune BT, Norman JM, Lazear HM, Artyomov M, Diamond MS, and Virgin HW (2015). Interferon-lambda cures persistent murine norovirus infection in the absence of adaptive immunity. Science 347, 269–273. 10.1126/science.1258100. [PubMed: 25431489]

Pimentel H, Bray NL, Puente S, Melsted P, and Pachter L (2017). Differential analysis of RNA-seq incorporating quantification uncertainty. Nature methods 14, 687–690. 10.1038/nmeth.4324. [PubMed: 28581496]

Reis BS, Hoytema van Konijnenburg DP, Grivennikov SI, and Mucida D (2014). Transcription Factor T-bet Regulates Intraepithelial Lymphocyte Functional Maturation. Immunity 41, 244–256. 10.1016/j.immuni.2014.06.017. [PubMed: 25148025]

Reis BS, Rogoz A, Costa-Pinto FA, Taniuchi I, and Mucida D (2013). Mutual expression of the transcription factors Runx3 and ThPOK regulates intestinal CD4(+) T cell immunity. Nature immunology 14, 271–280. 10.1038/ni.2518. [PubMed: 23334789]

Rogoz A, Reis BS, Karssemeijer RA, and Mucida D (2015). A 3-D enteroid-based model to study T-cell and epithelial cell interaction. Journal of immunological methods 421, 89–95. 10.1016/j.jim.2015.03.014. [PubMed: 25841547]

Sato T, Vries RG, Snippert HJ, van de Wetering M, Barker N, Stange DE, van Es JH, Abo A, Kujala P, Peters PJ, and Clevers H (2009). Single Lgr5 stem cells build crypt-villus structures in vitro without a mesenchymal niche. Nature 459, 262–265. nature07935 [pii] 10.1038/nature07935. [PubMed: 19329995]

Strong DW, Thackray LB, Smith TJ, and Virgin HW (2012). Protruding domain of capsid protein is necessary and sufficient to determine murine norovirus replication and pathogenesis in vivo. J Virol 86, 2950–2958. 10.1128/JVI.07038-11. [PubMed: 22258242]

Stuller KA, Cush SS, and Flano E (2010). Persistent gamma-herpesvirus infection induces a CD4 T cell response containing functionally distinct effector populations. Journal of immunology 184, 3850–3856. 10.4049/jimmunol.0902935.

Sujino T, London M, Hoytema van Konijnenburg DP, Rendon T, Buch T, Silva HM, Lafaille JJ, Reis BS, and Mucida D (2016). Tissue adaptation of regulatory and intraepithelial CD4(+) T cells controls gut inflammation. Science 352, 1581–1586. 10.1126/science.aaf3892. [PubMed: 27256884]

Swain SL, McKinstry KK, and Strutt TM (2012). Expanding roles for CD4(+) T cells in immunity to viruses. Nature reviews. Immunology 12, 136–148. 10.1038/nri3152.

Takeuchi A, and Hashimoto K (1976). Electron microscope study of experimental enteric adenovirus infection in mice. Infection and immunity 13, 569–580. 10.1128/iai.13.2.569-580.1976. [PubMed: 177370]

Tanoue T, Atarashi K, and Honda K (2016). Development and maintenance of intestinal regulatory T cells. Nature reviews. Immunology 16, 295–309. 10.1038/nri.2016.36.

Tinevez JY, Perry N, Schindelin J, Hoopes GM, Reynolds GD, Laplantine E, Bednarek SY, Shorte SL, and Eliceiri KW (2017). TrackMate: An open and extensible platform for single-particle tracking. Methods 115, 80–90. 10.1016/j.ymeth.2016.09.016. [PubMed: 27713081]

Tominaga K, Yoshimoto T, Torigoe K, Kurimoto M, Matsui K, Hada T, Okamura H, and Nakanishi K (2000). IL-12 synergizes with IL-18 or IL-1beta for IFN-gamma production from human T cells. International immunology 12, 151–160. 10.1093/intimm/12.2.151. [PubMed: 10653850]

Trombetta JJ, Gennert D, Lu D, Satija R, Shalek AK, and Regev A (2014). Preparation of Single-Cell RNA-Seq Libraries for Next Generation Sequencing. Current protocols in molecular biology 107, 4 22 21–17. 10.1002/0471142727.mb0422s107. [PubMed: 24984854]

Vacchio MS, Wang L, Bouladoux N, Carpenter AC, Xiong Y, Williams LC, Wohlfert E, Song KD, Belkaid Y, Love PE, and Bosselut R (2014). A ThPOK-LRF transcriptional node maintains the integrity and effector potential of post-thymic CD4+ T cells. Nature immunology 15, 947–956. 10.1038/ni.2960. [PubMed: 25129370]

van Leeuwen EM, Remmerswaal EB, Vossen MT, Rowshani AT, Wertheim-van Dillen PM, van Lier RA, and ten Berge IJ (2004). Emergence of a CD4+CD28− granzyme B+, cytomegalovirus-specific T cell subset after recovery of primary cytomegalovirus infection. Journal of immunology 173, 1834–1841. 10.4049/jimmunol.173.3.1834.

Wilen CB, Lee S, Hsieh LL, Orchard RC, Desai C, Hykes BL Jr., McAllaster MR, Balce DR, Feehley T, Brestoff JR, et al. (2018). Tropism for tuft cells determines immune promotion of norovirus pathogenesis. Science 360, 204–208. 10.1126/science.aar3799. [PubMed: 29650672]

Wilhelmi I, Roman E, and Sanchez-Fauquier A (2003). Viruses causing gastroenteritis. Clin Microbiol Infect 9, 247–262. 10.1046/j.1469-0691.2003.00560.x. [PubMed: 12667234]

Wilson SS, Bromme BA, Holly MK, Wiens ME, Gounder AP, Sul Y, and Smith JG (2017). Alpha-defensin-dependent enhancement of enteric viral infection. PLoS Pathog 13, e1006446. 10.1371/journal.ppat.1006446. [PubMed: 28622386]

Yoshimoto T, Takeda K, Tanaka T, Ohkusu K, Kashiwamura S, Okamura H, Akira S, and Nakanishi K (1998). IL-12 up-regulates IL-18 receptor expression on T cells, Th1 cells, and B cells: synergism with IL-18 for IFN-gamma production. Journal of immunology 161, 3400–3407.

Zaunders JJ, Dyer WB, Wang B, Munier ML, Miranda-Saksena M, Newton R, Moore J, Mackay CR, Cooper DA, Saksena NK, and Kelleher AD (2004). Identification of circulating antigen-specific CD4+ T lymphocytes with a CCR5+, cytotoxic phenotype in an HIV-1 long-term nonprogressor and in CMV infection. Blood 103, 2238–2247. 10.1182/blood-2003-08-2765. [PubMed: 14645006]

Highlights

- Viral infection results in the recruitment of intraepithelial $Ly6A^{+}CCR9^{+}CD4^{+}$ T cells
- IL-18 activates recruited intestinal $CD4^{+}$ T cells in the absence of TCR-stimulation
- Recruited $CD4^{+}$ T cells control viral replication via IFN-γ in a TCR-independent manner

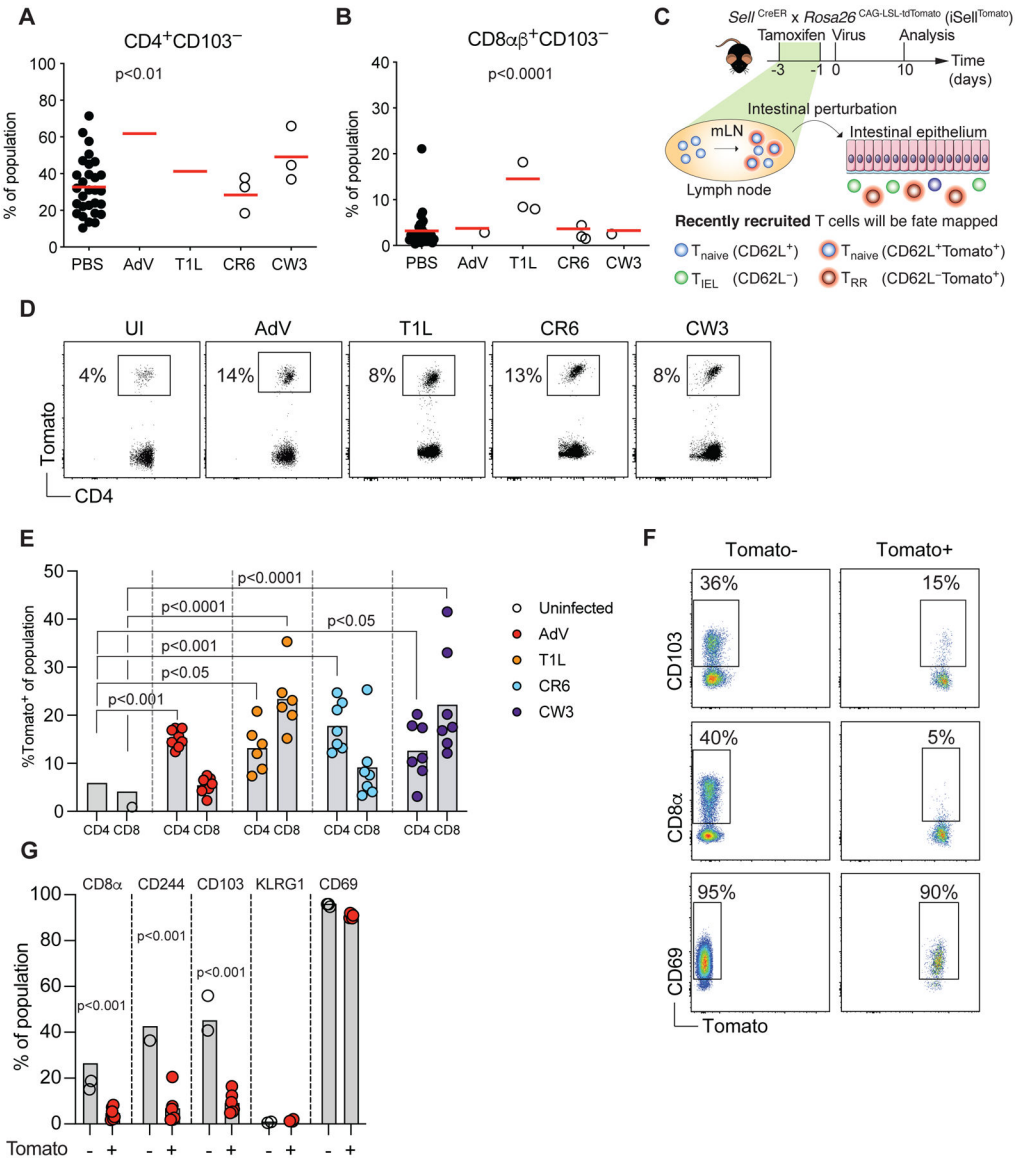

Figure 1. Distinct intraepithelial T cell dynamics post enteric viral infections.

(**A-B**) B6 mice were orally infected with 10^7 infectious units (i.u.) of murine adenovirus-2 (AdV), 10^8 plaque forming units (pfu) of reovirus T1L, 3×10^6 pfu of either murine norovirus (MNV) CR6 or CW3. $CD4^+CD103^-$ (**A**) or $CD8\alpha\beta^+CD103^-$ (**B**) small intestine intraepithelial lymphocytes (IEL) were analyzed 10 days post infection among total CD4 or CD8αβ T cells, respectively. (**C**) Experimental overview of the T cell fate-mapping model. $iSell^{Tomato}$ mice were treated orally with tamoxifen 1 and 3 days prior to viral infection, RR: recently recruited. (**D-E**) $iSell^{Tomato}$ mice were orally infected with 10^7 i.u. of AdV, 10^8 pfu of T1L, or 3×10^6 pfu of either CR6 or CW3, small intestine $TCR\beta^+CD4^+CD62L^-$ and $TCR\beta^+CD8\alpha\beta^+CD62L^-$ IELs were analyzed for tomato expression 10 days post infection. (**D**) Representative dot plots of tomato expression among $CD4^+$ IELs. (**E**) Frequencies of tomato expression among small intestine $CD4^+$ or $CD8^+$ IELs. (**F-G**) $iSell^{Tomato}$ mice were infected with 10^7 i.u. of AdV and expression of CD103, CD8α and CD69 were

analyzed among TCRβ^{+}CD4^{+}CD62L^{-}Tomato^{+} or Tomato^{-} cells. (**F**) Representative surface expression of markers as indicated among Tomato^{+} and Tomato^{-} T cells. (**G**) Frequencies of Tomato^{+} or Tomato^{-} cells expressing the indicated markers. Data are expressed as mean of individual mice in A and B (n = 6 for AdV, n = 5 for T1L, n = 12 for CR6, of two independent experiments, n = 3 for CW3, of one experiment), in E (n = 8 for AdV, n = 6 for CW3 and n = 7 for CR6 and T1L, of two independent experiments) and in G (n = 6 of two independent experiments). p values are as indicated, one-way ANOVA plus Bonferroni test in A and E, Student's t-test in G. See also Figure S1.

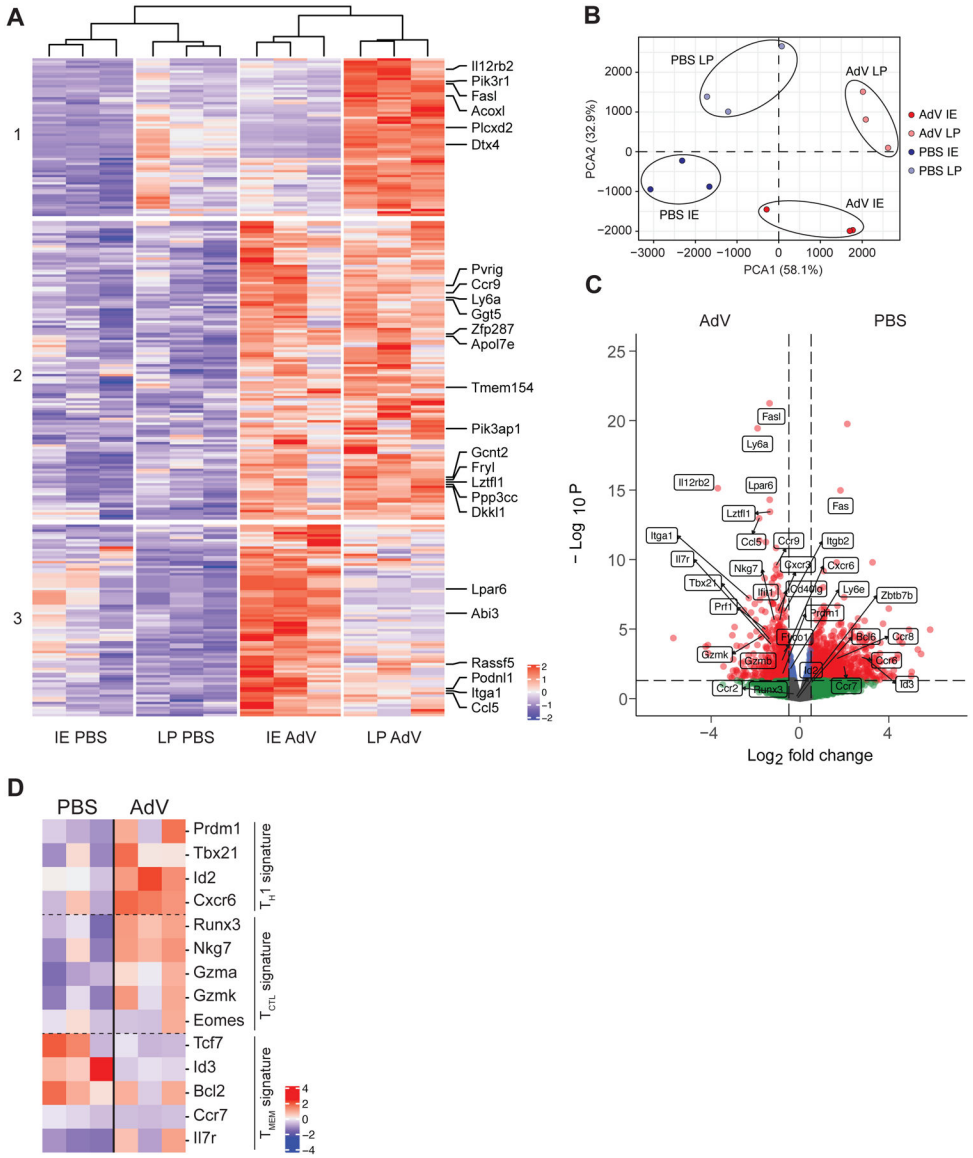

Figure 2. Transcriptional analysis of epithelial-recruited CD4$^+$ T cells post AdV-infection.

iSell^{Tomato} mice were infected with AdV or treated with PBS vehicle control, and CD4$^+$CD62L$^-$Tomato$^+$ T cells were sorted from small intestine lamina propria (LP) or intestinal epithelium (IE) 10 days post infection for bulk RNAseq. (**A**) Heatmap clustering of the most significant differentially expressed genes represented by normalized Z score in LP and IE of AdV-infected and PBS treated control mice. Top 25 genes are annotated. FDR < 0.05. (**B**) Principal component analysis of sorted T cells in IE and LP compartment of AdV-infected and control mice. (**C**) Volcano plot visualizing gene fold change (X-axis) versus p value (Y-axis) between T cells from AdV-infected and control mice for both IE and LP combined. Dashed line on y-axis denotes p value of 0.05 and dashed line on x-axis denotes fold change of ± 2. (**D**) Transcriptional signatures represented by normalized Z score of T cells between AdV-infected and control mice for both IE and LP combined. n = 3 mice per group from one experiment. Data are expressed as means of individual mice.

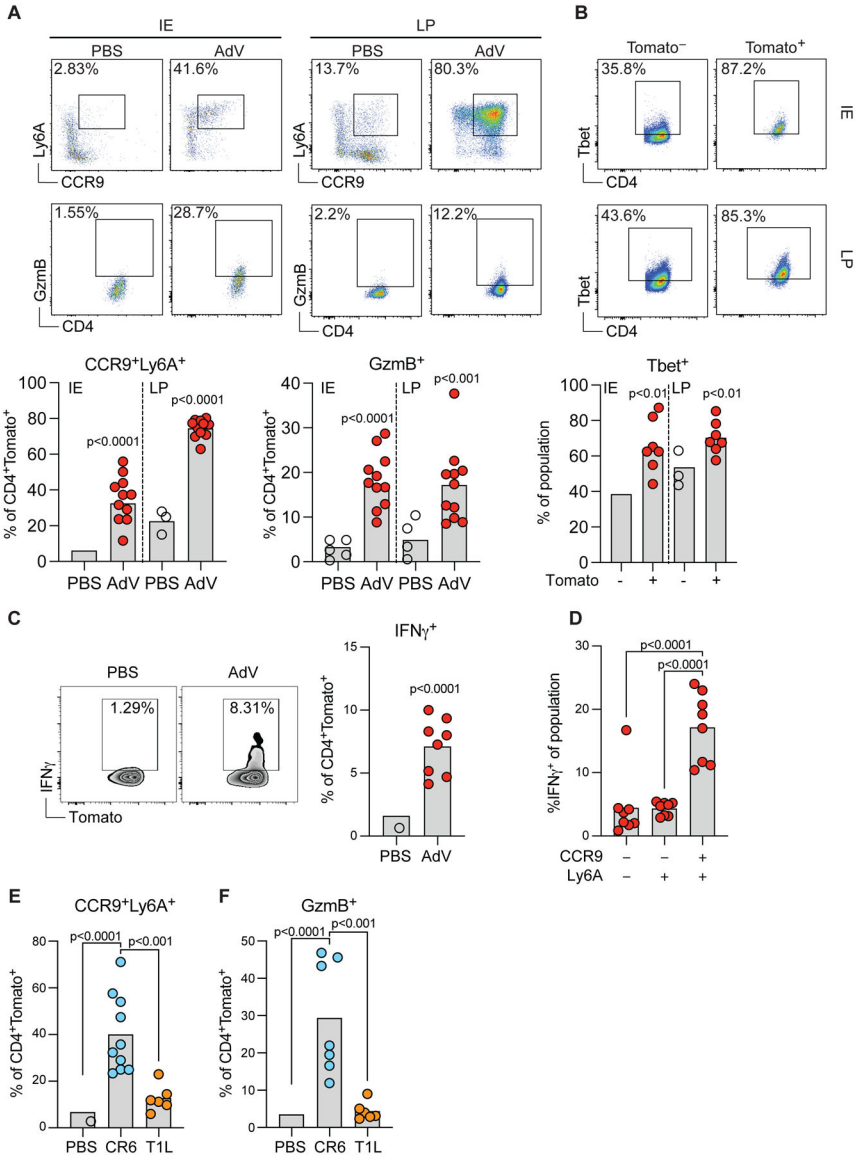

Figure 3. AdV- and CR6-recruited IE CD4$^+$ T cells are enriched for CCR9$^+$Ly6A$^+$ cells and acquire a Th1 and cytotoxic profile.

iSell^{Tomato} mice were infected with AdV or treated with PBS vehicle only, and small intestine CD4$^+$CD62L$^-$Tomato$^+$ T cells were analyzed 10 days post infection (**A-D**). (**A**) Representative plots (top) of marker expression and population frequencies (bottom) as indicated among CD4$^+$CD62L$^-$Tomato$^+$ T cells in LP or IE compartments. (**B**) Representative plots (top) and frequencies (bottom) of T-bet expression among Tomato$^+$ or Tomato$^-$ cells in IE and LP. (**C**) Representative plots (left) and frequencies (right) of IFN-γ production among CD4$^+$CD62L$^-$Tomato$^+$ T cells in the IE. (**D**) Frequencies of IFN-γ production among CCR9$^-$Ly6A$^-$, Ly6A$^+$CCR9$^-$ and CCR9$^+$Ly6A$^+$ cells within CD4$^+$Tomato$^+$ T cells. (**E-F**) iSell^{Tomato} mice were infected with CR6 or T1L, or treated with PBS vehicle only, and CD4$^+$CD62L$^-$Tomato$^+$ T cells was analyzed for Ly6A, CCR9 (**E**) and GzmB (**F**) expression 10 days post infection among CD4$^+$CD62L$^-$Tomato$^+$ cells. Data are expressed as means of individual mice, for A (n = 10 for control and n = 11

for AdV, of two independent experiments), for B (n = 7 of two independent experiments), for C and D (n = 8 of two independent experiments), for E (n = 6–10, two independent experiments), and for F (n = 6–10, two independent experiments). p values are as indicated, Student's t-test in A, B and C. One-way ANOVA plus Bonferroni test in D, E and F. See also Figure S2, S3 and S4.

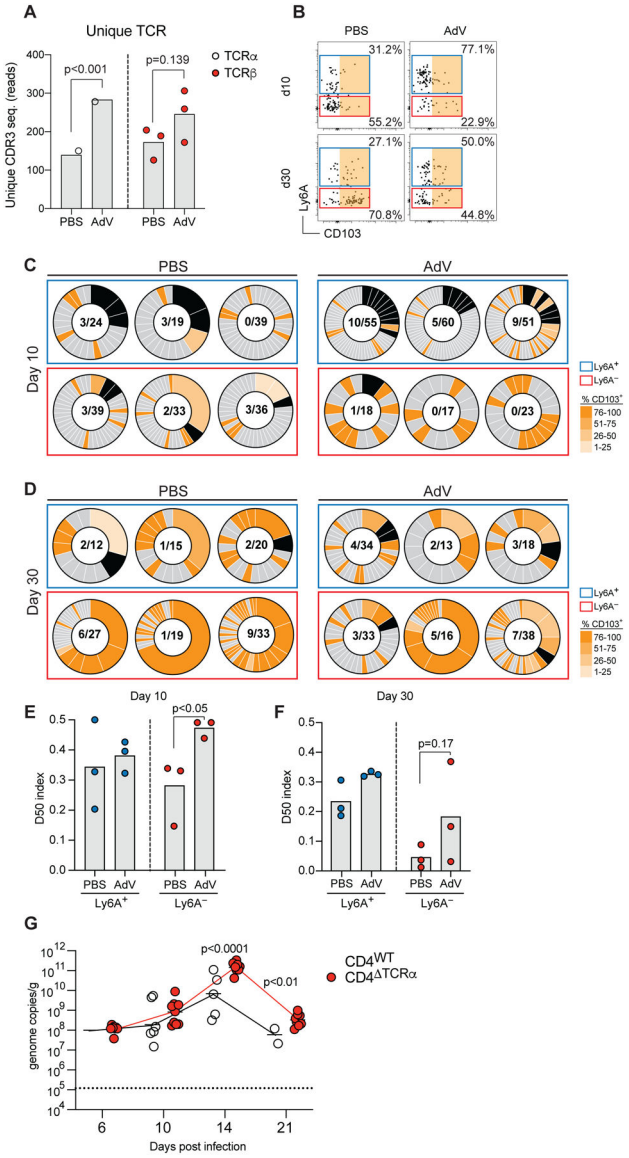

Figure 4. Clonally diverse Ly6A^{+}CD4^{+} T cells are recruited to the IE compartment 10- and 30-days post AdV-infection.

(**A**) Unique TCRα and TCRβ CDR3 sequence reads were extracted from bulk RNAseq data in figure 2. **(B-F)** iSell^{Tomato} mice were infected with AdV or treated with PBS vehicle control only, and small intestine CD4^{+}CD62L^{-}Tomato^{+} T cells were single-cell sorted at 10- and 30-days post infection for TCRβ-seq. (**B**) Ly6A and CD103 expression analysis of CD4^{+}CD62L^{+}Tomato^{+} T cells indexed and sorted for analysis in B and C. Colored gates represent indexed analysis in B and C. Orange area indicates CD103^{+} gate for C and D. Single cell TCRβ analysis at day 10 (**C**) and day 30 (**D**) post AdV-infection. Box colors represent gate color in A. Black pie regions represent expanded clones, grade of orange represents level of CD103 expression per clone indexed in A. Nominator represents total number of expanded clones, denominator represent total number of sequenced clones. (**E-F**) D50 analysis of CD4^{+}Tomato^{+}Ly6A^{+} and Ly6A^{-} at day 10 (**E**) and day 30 (**F**) post AdV infection. (**G**) Viral genome copies of AdV per gram of feces of AdV-infection over time of

iCD4$^{\Delta TCR\alpha}$ mice, dashed line represents limit of detection. Data are expressed as mean of individual mice, for A (n = 3 per group and timepoint, 1 experiment), for B-F (n = 3 per group and timepoint, 1 experiment), and for G (n = 8–12, two independent experiments). Significant p values as indicated, Student's t-test in A, E, F and G. See also Figure S4.

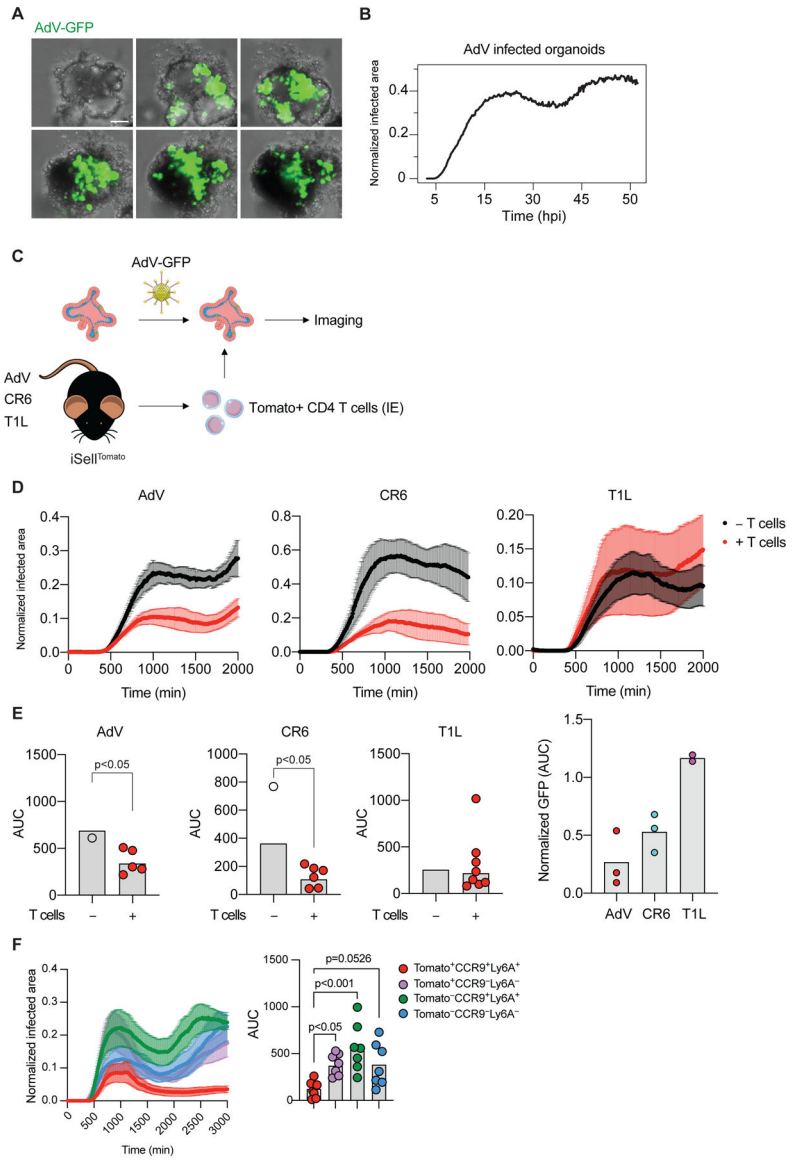

Figure 5. Newly recruited IE CD4^{+} T cells show anti-viral activity in AdV-infected intestinal organoid co-cultures.

(**A-B**) Small intestinal organoids were infected with 10^4 i.u. of AdV-GFP and imaged for 48 hours. (**A**) Representative images of organoids infected with AdV-GFP (green) at the indicated times post infection (hours, top left corner). (**B**) GFP expression area over time normalized to the area of organoids. (**C-E**) iSell^{Tomato} mice were infected with different viruses, small intestine CD4^{+}Tomato^{+} IE T cells were then sorted and co-cultured with 10^4 i.u. AdV-GFP infected organoids. (**C**) Experimental overview. (**D**) Representative graphs of GFP expression area from AdV-GFP infected organoids normalized to the area of the organoids over time with (red) or without (black) CD4^{+}Tomato^{+} IE T cells derived from mice infected with AdV, CR6 or T1L 10 days post infection. Data are expressed as mean ± SEM of individual experiment. (**E**) Summarized area under the curve (AUC) for D. Data points for individual organoids in E (left). Pooled data from 2–3 experiments (right). (**F**) iSell^{Tomato} mice were infected with AdV, CD4^{+}Tomato^{+}CCR9^{+}Ly6A^{+},

$CD4^+Tomato^+CCR9^-Ly6A^-$, $CD4^+Tomato^-CCR9^+Ly6A^+$ and $CD4^+Tomato^-CCR9^-Ly6A^-$ IE T cells were then sorted and co-cultured with 10^4 i.u. AdV-GFP infected organoids. Data are expressed as mean of individual organoid in E (except right figure of pooled data) and F. n = 5–10 organoids of two independent experiments A-E, one experiment in F. p values as indicated, Student's t-test in E or one-way ANOVA plus Bonferroni test in F.

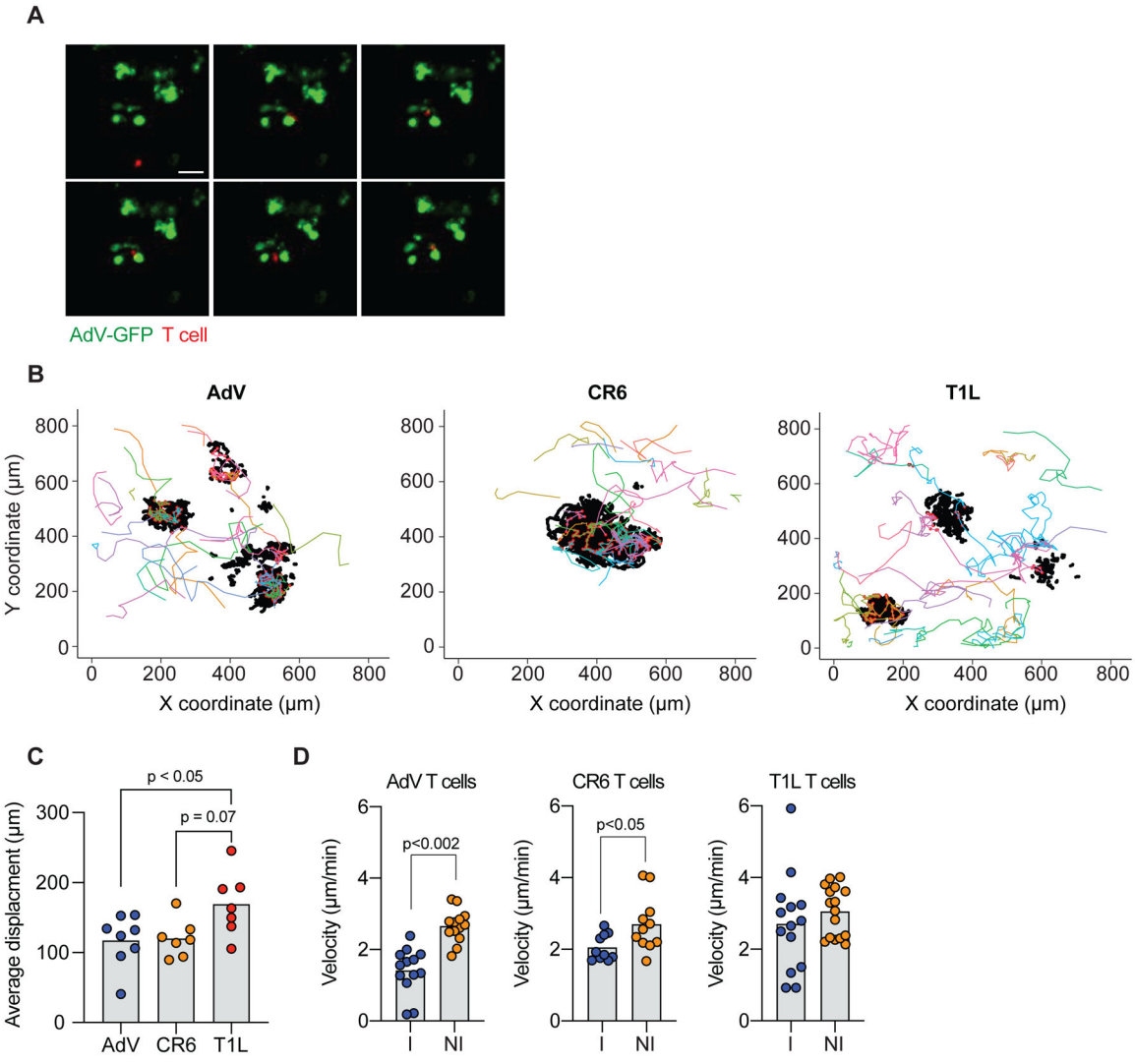

Figure 6. Newly recruited IE CD4$^+$ T cells interact with AdV-infected epithelial cells in intestinal organoids.

(**A-D**) Small intestine CD4$^+$Tomato$^+$ IE T cells derived from AdV, CR6 or T1L infected iSell^{Tomato} mice were co-cultured with AdV-GFP infected organoids and tracked over 48 ± 2 hours. (**A**) Representative images of AdV-GFP infected organoids (green) and IE CD4$^+$Tomato$^+$ T cells (red) derived from AdV-infected mice. Arrows indicate tracked T cells, top left corner indicates time post infection in minutes. (**B**) Tracking was obtained in 3 dimensions (x, y, and z); figure shows only x and y. Each colored line represents a unique T cell track, black dots represent GFP$^+$ epithelial cells and red dots represent T cell-organoid interaction points (<20 μm radius distance). (**C**) Average displacement distance of tracked Tomato$^+$ T cells co-cultured with AdV-infected organoids. (**D**) Velocity of tracked tomato$^+$ T cells, interacting T cells (I) within 20 μm radius of GFP$^+$ cells, or non-interacting (NI) T cells outside the 20 μm radius of GFP$^+$ cells. Data are expressed as mean of individual organoid in C (n = 7–8, two independent experiments). Data are expressed as average of pooled T cell tracks in D (n = 10–16 of two independent experiments). p values as indicated, One-way ANOVA plus Bonferroni test in C, Student's t-test in D.

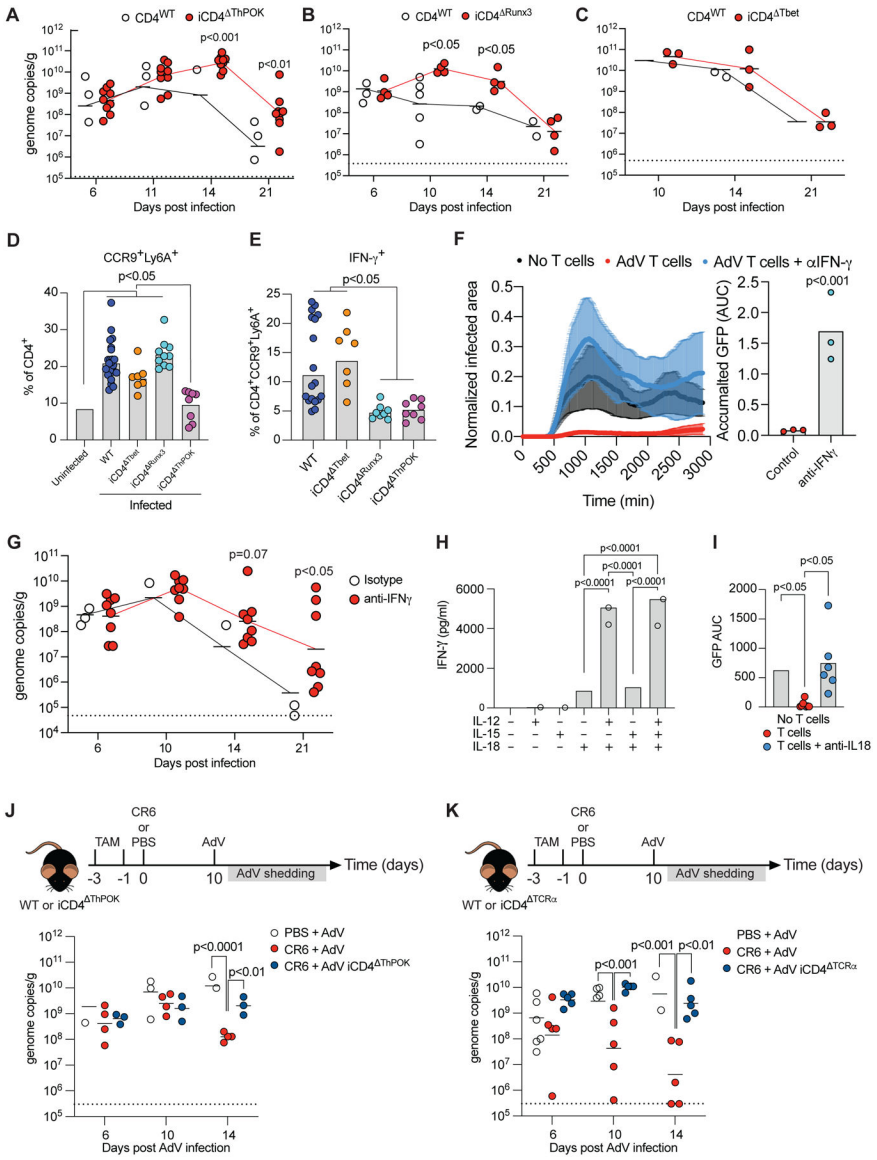

Figure 7. ThPOK-dependent CCR9^{+}Ly6A^{+} CD4^{+} T cells show anti-adenoviral function *in vivo*.

(A-C) AdV genome copies per gram of feces over time of post-infection (**A**) iCD4$^{\Delta ThPOK}$, (**B**) or iCD4$^{\Delta Runx3}$ (**C**) iCD4$^{\Delta Tbet}$ mice. Dashed line represents limit of detection. (**D-E**) Mice were infected with AdV and small intestine IE T cells were analyzed 10 days post infection. (**D**) Frequency of CCR9^{+}Ly6A^{+} cells among CD4^{+} T cells. (**E**) IFN-γ production among CCR9^{+}Ly6A^{+}CD4^{+} T cells. (**F, I**) iSell^{Tomato} mice were infected with AdV and small intestine CD4^{+}Tomato^{+} T cells were sorted at day 10 post infection. T cells was co-cultured with AdV-GFP infected organoids and imaged with or without anti-IFN-γ (**F**) or anti-IL-18 (**I**) blocking antibodies. Normalized infected area over time imaged (left) and accumulated GFP protein expression (right) in indicated conditions. (**G**) AdV genome copies per gram of feces over time in mice treated with IFN-γ blocking antibody or isotype control at day 8, 10, 12, 14, 16 and 18 post infection. (**H**) iSell^{Tomato} mice were infected with AdV and small intestine CD4^{+}Tomato^{+} T cells were sorted at day 10 post infection.

T cells was cultured and stimulated with IL-12, IL-15 and IL-18 as noted in figure for 24 hours. (**J-K**) WT, iCD4$^{\Delta ThPOK}$ or iCD4$^{\Delta TCR\alpha}$ mice were infected with CR6 (or PBS as control) and infected with AdV 10 days later. AdV stool shedding was measured post AdV-infection. Dashed line represents limit of detection. AdV genome copies per gram of stool of iCD4$^{\Delta ThPOK}$ (**I**) or iCD4$^{\Delta TCR\alpha}$ (**J**) mice relative to WT controls over time. Data are expressed as mean of individual mice in A, B, C, D, E, G, J and K, and F and I is expressed as mean of individual organoids, for A (n = 7–9, two independent experiments), for B (n = 4–5, one experiment), for C (n = 3–5, one experiment), for D and E (n = 7–18, two independent experiments), for G (n = 6–8, two independent experiments), for H (n = 2–3, representative of two independent experiments), for I (n = 6–9, one experiment), for J (n = 3–5, one experiment), for K (n = 5–10, two independent experiments). p values as indicated, one-way ANOVA plus Bonferroni test in D, E, H, I, J (log10 transformed) and K (log10). Student t-test in A (log10), B (log10), C (log10), F and G (log10). See also Figure S5.

KEY RESOURCES TABLE

REAGENT or RESOURCE	SOURCE	IDENTIFIER
Antibodies		
APC anti-mouse IL-18Ra (clone: A17071D)	Thermo Fisher Scientific	Cat# 157905, RRID:AB_2860734
Alexa Fluor 700 anti-mouse CD4 (clone: RM4–5)	BD Biosciences	Cat# 557956, RRID:AB_396956
APC anti-mouse IFNg (clone: XMG1.2)	Thermo Fisher Scientific	Cat# 25-7311-82, RRID:AB_469680
BV605 anti-mouse CD8a (clone: 53–6.7)	BioLegend	Cat# 100744, RRID:AB_2562609
BV711 anti-mouse CD8b (clone: H35–17.2)	BD Biosciences	Cat# 740761, RRID:AB_2740424
APC anti-mouse CD8b (clone: H35–17.2)	Thermo Fisher Scientific	Cat# 17-0083-81, RRID:AB_657760
PE-Cy7 anti-mouse CD45 (clone: 30-F11)	Thermo Fisher Scientific	Cat# 25-0451-82, RRID:AB_2734986
eFluor 450 anti-mouse granzyme B (clone: NGZB)	Thermo Fisher Scientific	Cat# 48-8898-82, RRID:AB_11149362
BV421 anti-mouse CD103 (clone: 2E7)	BioLegend	Cat# 121421, RRID:AB_10900074
eFluor 450 anti-mouse CD62L (clone: MEL-14)	Thermo Fisher Scientific	Cat# 48-0621-82, RRID:AB_1963590
FITC anti-mouse CD69 (clone: AB_465120)	Thermo Fisher Scientific	Cat# 11-0691-85, RRID:AB_1134101
APC anti-mouse TCRb (clone: H57–597)	Thermo Fisher Scientific	Cat# 17-5961-83, RRID:AB_469482
APCef780 anti-mouse TCRb (clone: H57–597)	Thermo Fisher Scientific	Cat# 47-5961-82, RRID:AB_1272173
PerCP-eFluor710 anti-mouse TCRgd (clone: GL-3, GL3)	Thermo Fisher Scientific	Cat# 46-5711-82, RRID:AB_2016707
BV421 anti-mouse CCR9 (clone: CW-1.2)	BD Biosciences	Cat#: 565412 RRID: AB_2739223
FITC anti-mouse Ly6A (clone: D7)	Biolegend	Cat# 108106, RRID:AB_313342
Alexa Fluor 647 anti-mouse CD244.2 (clone: eBio244F4)	Thermo Fisher Scientific	Cat# 51-2441-82, RRID:AB_657870
V450 anti-mouse/human Tbet (clone: O4–46)	BD Biosciences	Cat#: 561312 RRID:AB_10611714
APC anti-mouse CD5 (clone: 53–7.3)	Thermo Fisher Scientific	Cat#: 17-0051-81 RRID: AB_469330
Aqua fluorescent reactive dye	TheromoFisher Scientific	Cat# 34966
PE or APC TL (T3b) Tetramer	NIH tetramer facility	Not applicable
PE or APC LLO Tetramer	NIH tetramer facility	Not applicable
Anti-mouse IFNg (clone: XMG1.2)	BioXcell	Cat#: BE0055 RRID: AB_1107694
Anti-mouse IL-18 (clone: YIGIF74–1G7)	BioXcell	Cat#: BE0237 RRID: AB_2687719
Rat IgG1 (clone: HRPN)	BioXCell	Cat#: BE0088 RRID: AB_1107775
Rat IgG2a (clone: 2A3)	BioxCell	Cat#: BE0089 RRID: AB_1107769
Bacterial and Virus Strains		
Murine Adenovirus-2	Provided by J. Smith	Wilson et al., 2017
Listeria monocytogenes 10403S-inlA expressing full length OVA	Provided by L. Lefrançois	Sheridan et al., 2014
Reovirus T1L	Provided by B. Jabri	Bouziat et al., 2017
Murine norovirus CW3	Provided by K. Cadwell	Kernbauer et al, 2014
Murine norovirus CR6	Provided by K. Cadwell	Kernbauer et al, 2014
Murine Adenovirus-2-GFP	Provided by J. Smith	Wilson et al., 2017
Biological Samples		
Chemicals, Peptides, and Recombinant Proteins		

REAGENT or RESOURCE	SOURCE	IDENTIFIER
Tamoxifen	Sigma-Aldrich	Cat# T5648
Ionomycin	Sigma-Aldrich	Cat# I0634
GolgiStop with Monensin	BD Biosciences	Cat# 554724
Dithiothreitol (DTT)	Sigma-Aldrich	Cat# 10197777001
Phorbol 12-myristate 13-acetate (PMA)	Sigma-Aldrich	Cat#: P8139
EDTA	ThermoFisher Scientific	Cat# AM9260G
Percoll	GE Healthcare	Cat# 17-0891-01
Streptomycin Sulphate	MP Biomedicals	Cat# 0219454125
Oxford Listeria selective agar base	Sigma Aldrich	Cat# 1070040500
Oxford Listeria selective supplement	Sigma Aldrich	Cat# 1070060010
TCL buffer	Qiagen	Cat# 1031576
RNAClean XP beads	Agentcourt	Cat# A63987
Maxima H- reverse transcriptase (RT)	ThermoFisher Scientific	Cat# EP0751
Betaine Solution	Millipore Sigma	Cat# B0300
RNAsin Plus RNase Inhibitor	ThermoFisher Scientific	Cat# PRN2615
CytoFix/CytoPerm Fixation/Permeabilization Solution Kit	BD Biosciences	Cat# 554714
Saponin	Sigma Aldrich	Cat# 47036
RPMI 1650	Gibco	Cat# 21870076
Fetal Bovine Serum	Sigma	Cat# F0926
Pen/Strep	Gibco	Cat# 10378016
L-glutamine	Gibco	Cat# 25030–081
Sodium Pyruvate	Gibco	Cat# 11360070
Non-essential amino acids	Gibco	Cat# 11140050
2-mercaptoethanol	Sigma	Cat# M3148
HEPES	Gibco	Cat# 15630–080
Corn Oil	Sigma-Aldrich	Cat# C8267
R-spondin	R&D	Cat# 4645-RS
Noggin	Peprotech	Cat# 250–38
EGF	Peprotech	Cat# 315–09
IL-2	R&D	Cat# 402-ML
IL-15 complex	ThermoFisher Scientific	Cat# 16-8156-82
IL-7	R&D	Cat# 407-ML
IL-18	R&D	Cat# 9124-IL
IFN-g	R&D	Cat# 485-MI
Matrigel	ThermoFisher Scientific	Cat# CB40230A
Critical Commercial Assays		
eBioscience™ Foxp3 / Transcription Factor Staining Buffer Set	Thermo Fisher Scientific	Cat# 00-5523-00
LIVE/DEAD™ Fixable Aqua Dead Cell Stain Kit	Thermo Fisher Scientific	Cat# L34966
Miseq Reagent Kit v2 (500 cycles)	Illumina	Cat# MS-103–1003

REAGENT or RESOURCE	SOURCE	IDENTIFIER
Nextera XT DNA Library Preparation Kit (24 samples)	Illumina	Cat# FC-131–1024
QIAamp Fast DNA Stool Mini Kit	Qiagen	Cat# 51604
PowerSYBR Green	Applied Biosystems	Cat# 4368577
IFN-γ ELISA	Thermo Fisher Scientific	Cat# 88-7314-88
IL-18 ELISA	Thermo Fisher Scientific	Cat# 88-50618-88
Deposited Data		
Bulk RNA-Seq	This paper	GEO: GSE196417
Single cell TCR seq	This paper	GEO: GSE196417
Experimental Models: Cell Lines		
Experimental Models: Organisms/Strains		
Mouse: Sell-CreER	Provided by M. Nuzzensweig	Merkenschlager et al., 2021
Mouse: B6.129S2-H2$^{dlAb1\text{-}Ea}$/J	Jackson Laboratory	Jax: 003584
Mouse: *Thpok*^{eGFP}: B6.129P2(Cg)-*Zbtb7b*^{tm2Litt}/J	Jackson Laboratory	Jax: 027663
Mouse: *Rosa26*$^{lsl\text{-}tdTomato}$: B6.Cg-*Gt(ROSA)26Sor*$^{tm14(CAG\text{-}tdTomato)\ Hze}$/J	Jackson Laboratory	Jax: 007914
Mouse: *Trac*$^{f/f}$	Provided by A. Rudensky, (MSKCC)	Bilate et al., 2020
Mouse: Runx3$^{f/f}$	Jackson Laboratory	Jax: 008773
Mouse: Tbx21$^{f/f}$	Jackson Laboratory	Jax: 022741
Mouse: Zbtb7b$^{f/f}$	Jackson Laboratory	Jax: 009369
Mouse: Ifngr1$^{-/-}$	Jackson Laboratory	Jax: 003288
Oligonucleotides		
Biotinylated-T22VN used for Bulk RNAseq RT/cDNA synthesis: 5’- Bio-TTTTTTTTTTTTTTTTTTTTTTVN - 3’	Integrated DNA Technologies	Not applicable
All TCR and barcode primers used for scTCRseq are found in Table S1.	Integrated DNA Technologies	Bilate et al., 2020
Paired-end (PE) P1 used for scTCRseq by Miseq 5’-AATGATACGGCGACCACCGAGATCTACACTCTTTCCCTACACGACGCTCTTCCGATCT -3’	Integrated DNA Technologies	Han et al., 2014
PE P2 used for scTCRseq by Miseq 5’-AAGCAGAAGACGGCATACGAGATCGGTCTCGGCATTCCTGCTGAACCGCTCTTCCGATCT -3’	Integrated DNA Technologies	Han et al., 2014
Adenovirus FW 5’-GTCCGATTCGGTACTACGGT-3’	Integrated DNA Technologies	Gounder, A.P et al., 2016
Adenovirus RV 5’-GTCAGACAACTTCCCAGGGT-3’	Integrated DNA Technologies	Gounder, A.P et al., 2016
Recombinant DNA		
Software and Algorithms		
GraphPad Prism 9.0	GraphPad	https://www.graphpad.com/scientific-software/prism/
FlowJo v 10	BD Biosciences	https://www.flowio.com/solutions/flowio

REAGENT or RESOURCE	SOURCE	IDENTIFIER
FACSDiva	BD Biosciences	https://www.bdbiosciences.com/en-us/instruments/research-instruments/research-software/flow-cytometry-acquisition/facsdiva-software
IMGT	Brochet et al., 2008	imgt.org/HighV-QUEST
R	Not applicable	https://cran.r-project.org/
PANDASEQ	Masella et al., 2012	https://github.com/neufeld/pandaseq
sleuth (v0.30) package for R	Pimentel et al., 2017	https://github.com/pachterlab/sleuth
kallisto (v0.46) software	Bray et al., 2016	https://github.com/pachterlab/kallisto
Immunarch (v0.6.5) package	Not applicable	10.5281/zenodo.3893991)
ImageJ	Not applicable	https://imagej.nih.gov/ij/
TrackMate 6.0.2	Tinevez et al., 2017	https://imagej.net/plugins/trackmate/
QuantStudio 3 RT PCR System	Applied Biosystems	https://www.thermofisher.com/us/en/home/life-science/pcr/real-time-pcr/real-time-pcr-instruments/quantstudio-systems.html
Other		